3-16-2015

Multi-episodic Remagnetization Related to Deformation in the Pyrenean Internal Sierras

Esther Izquierdo-Llavall

Antonio Casas Sainz

Belén Oliva-Urcia

Russ F. Burmester
Western Washington University, russ.burmester@wwu.edu

Emilio L. Pueyo

See next page for additional authors

Recommended Citation

Esther Izquierdo-Llavall, Antonio Casas Sainz, Belén Oliva-Urcia, Russell Burmester, Emilio L. Pueyo, Bernard Housen; Multi-episodic remagnetization related to deformation in the Pyrenean Internal Sierras, Geophysical Journal International, Volume 201, Issue 2, 1 May 2015, Pages 891–914, https://doi.org/10.1093/gji/ggv042

Geophysical Journal International

Geophys. J. Int. (2015) **201,** 891–914 doi: 10.1093/gji/ggv042

GJI Geomagnetism, rock magnetism and palaeomagnetism

Multi-episodic remagnetization related to deformation in the Pyrenean Internal Sierras

Esther Izquierdo-Llavall,[1] Antonio Casas Sainz,[1] Belén Oliva-Urcia,[2] Russell Burmester,[3] Emilio L. Pueyo[4] and Bernard Housen[3]

[1] *Departamento de Ciencias de la Tierra, Universidad de Zaragoza, E-*50009 *Zaragoza, Spain. E-mail: estheriz@unizar.es*
[2] *Departamento de Geología y Geoquímica, Universidad Autónoma de Madrid, E-*28049 *Madrid, Spain*
[3] *Department of Geology, Western Washington University,* 516 *High St. MS* 9080*, Bellingham, WA* 98225*, USA*
[4] *Instituto Geológico y Minero de España, Oficina de Zaragoza c/ M. Lasala,* 44*, E-*50006 *Zaragoza, Spain*

Accepted 2015 January 20. Received 2015 January 15; in original form 2014 July 8

SUMMARY

The Internal Sierras (IS) in the southern margin of the Western and Central Axial Zone (Southern Pyrenees) are affected by a syn-orogenic remagnetization that provides information to reconstruct deformation geometries at the time of acquisition of magnetization. Furthermore, the IS structure changes strike along its structural trend, from ∼N120 to 130°E in the western and eastern margins to ∼N070–090°E in the central part. Palaeomagnetic techniques have been used to (i) accurately define the timing of remagnetization with regard to deformation and (ii) determine if the along-strike trend variation in the IS was induced by deformation and thrust emplacement during the Pyrenean compression or, on the contrary, was the result of a primary orientation controlled by structures inherited from pre-orogenic times. From 23 new palaeomagnetic sites, collected in Upper Cretaceous marls and marly limestones, two meaningful and stable palaeomagnetic components were resolved, principally carried by magnetite: (1) a lower-temperature component (B) that unblocks between 200 °C and 325–400 °C and (2) a higher-temperature component (C) that has been successfully isolated by means of combined thermal (up to 400 °C) and AF demagnetization (generally up to 50–100 mT). The B component is a late remagnetization that post-dates folding and emplacement of basement thrust sheets in the IS (mainly the Gavarnie thrust). It supports small but statistically significant clockwise rotations in the western part of the IS (from +18 to +26°). These rotations can be attributed to the westwards shortening decrease in the thrust system below the Gavarnie unit that results from its along-strike structural change, with a higher number of basement thrusts to the east. The C component has been interpreted as an early remagnetization, based on the results of conglomerate and fold tests. This component predates basement thrusting and is diachronous across the study area: reverse and normal polarities dominate in the eastern and western margins of the IS, respectively. New and previous palaeomagnetic data point out that curvature in the IS is probably a primary feature and the along-strike change in their trend could be interpreted as the result of basement geometrical features inherited from Variscan, Late Variscan or Mesozoic times. A complex, multi-episodic remagnetization probably related to burial and deformation processes occurred during Eocene times.

Key words: Palaeomagnetism applied to tectonics; Palaeomagnetism applied to geological processes; Remagnetization; Continental tectonics: compressional.

1 INTRODUCTION

The combination of palaeomagnetic and classical structural studies has been widely applied to the reconstruction of orogen curvature and kinematic evolution of fold and thrust systems (Sussman & Weil 2004; Weil & Sussman 2004). On the one hand, palaeomagnetic techniques are commonly used to quantify vertical axis rotations (VARs) related to orocline development, lateral gradients of thrust displacement or simple shear deformation (Schwartz & Van der Voo 1983; Allerton 1998; Sussman & Weil 2004; Soto *et al.* 2006; Weil *et al.* 2010). Particularly, in arcuate fold and thrust systems, palaeomagnetism is useful in order to determine whether curved

geometries are primary (normally resulting from the inversion of a previous irregular fault or basin geometry) or secondary (formed by bending of an initially linear structure about a vertical axis) (Weil & Sussman 2004; Weil *et al.* 2010). On the other hand, another (not so common) aim of the interpretation of palaeomagnetic components is to determine structural deformations about horizontal fold axis, especially where no palaeohorizontal markers exist (McClelland & McCaig 1989; Villalaín *et al.* 2003; Soto *et al.* 2011).

Remagnetizations are relatively common in rocks subject to thrusting during orogenic evolution (these remagnetizations may be either post- or syn-orogenic, during a particular deformation stage or between two tectonic phases; Stamatakos *et al.* 1996; Enkin *et al.* 2000; Lewchuk *et al.* 2002; Oliva-Urcia *et al.* 2008; Szabó & Cioppa 2012; Zechmeister *et al.* 2012). Syn-orogenic remagnetized components are extremely interesting from the structural point of view because they enable recovery of the shape and orientation of compressional structures at the time of the magnetic overprinting (Stamatakos & Hirt 1994; Jordanova *et al.* 2001; Lewchuk *et al.* 2002; Henry *et al.* 2004; Weil & Sussman 2004; Pueyo *et al.* 2007). With regard to the study of vertical and horizontal axis rotations, syn-orogenic remagnetizations make difficult the direct interpretation of paleomagnetic data and require an accurate understanding of the age of acquisition of the remagnetization. It is important to note that remagnetization components which completely replace the primary signal allow quantification of rotations that occurred after the remagnetization event, but the rotational history predating remagnetization cannot be obtained from those palaeomagnetic vectors.

In the Pyrenean range, results from a large number of palaeomagnetic studies carried out in the past decades document differential VARs as well as common development of syn-orogenic remagnetizations (Bates 1989; Dinarès *et al.* 1992; Pueyo *et al.* 2002, 2004; Sussman *et al.* 2004; Oliva-Urcia & Pueyo 2007; Oliva-Urcia *et al.* 2010; Mochales *et al.* 2012; Muñoz *et al.* 2013; Rodríguez-Pintó *et al.* 2013). Several studies have focused on the rotation of structures within the Mesozoic–Cenozoic sedimentary cover (Mochales *et al.* 2012; Muñoz *et al.* 2013 and references therein), where it is easier to constrain the age of rotation from syn-tectonic sediments, but these sedimentary units are absent in the internal zones of the chain. In the central-western part of the Pyrenean Axial Zone (where this study is focused, see location in Fig. 1a), previous palaeomagnetic studies have been carried out mainly in the Permian–Triassic and Upper Cretaceous cover units cropping out in its southern and northern margins (Van der Lingen 1960; Schwarz 1963; Cogné 1987; Bates 1989, Oliva-Urcia 2004; Oliva-Urcia & Pueyo 2007; Oliva-Urcia *et al.* 2008, 2012; Izquierdo-Llavall *et al.* 2014). The resulting large data set indicates moderate (between 10 and 20°), occasionally strong (up to +45°) mean rotations, as well as frequently developed syn-orogenic remagnetizations.

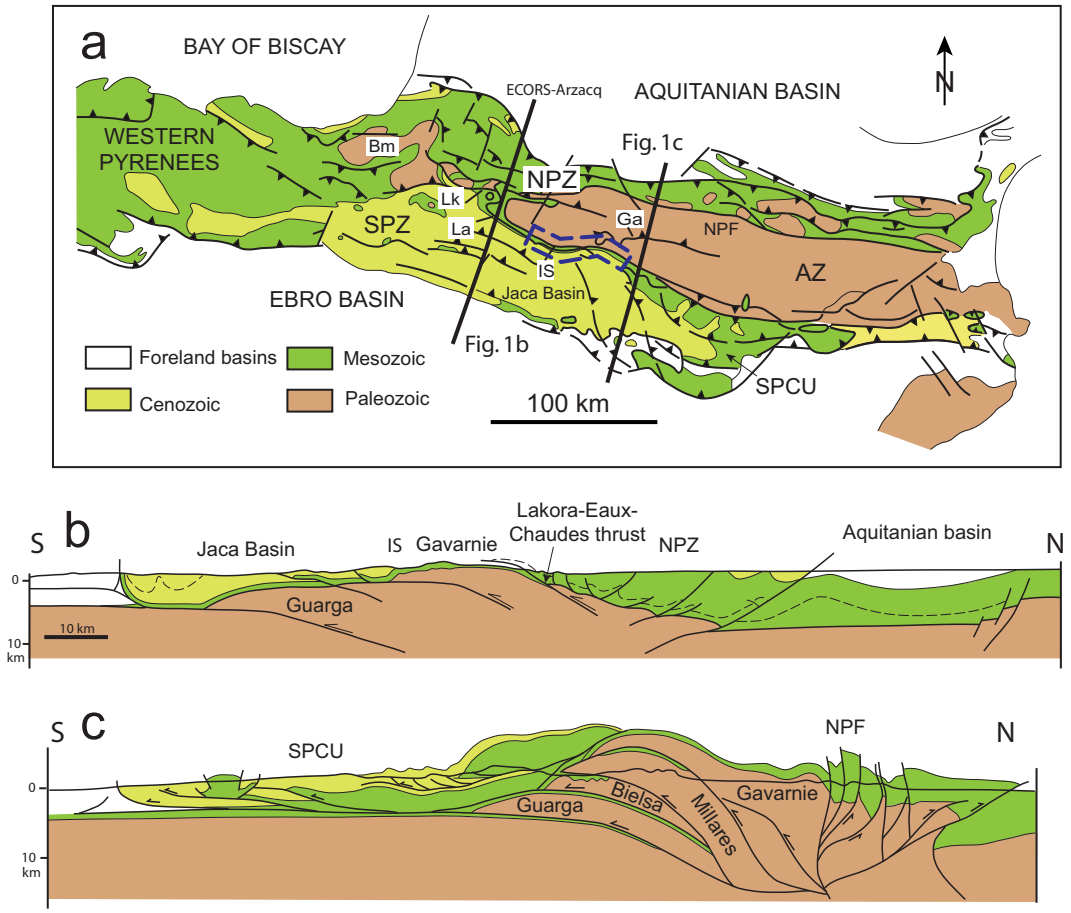

Figure 1. (a) Geological sketch of the Pyrenees (modified from Teixell 1996) with location of the study area. BM, Basque Massifs; Lk, Lakora-Eaux-Chaudes thrust; La, Larra-Monte-Perdido thrust system; IS, Internal Sierras; NPZ, North Pyrenean Zone; Ga, Gavarnie thrust; NPF, North Pyrenean Fault; SPCU, South Pyrenean Central Unit; AZ, Axial Zone. Geological, range-scale cross sections across the (b) western (modified from Teixell 1998) and (c) eastern margins (modified from Martínez-Peña & Casas-Sainz 2003) of the study area.

The present project is the structural and palaeomagnetic study of the Upper Cretaceous cover of the Pyrenean Axial Zone that crops out in the Internal Sierras (IS; Fig. 1a). This structural domain shows, in map view, an intriguing feature: an along-strike change in its structural trend, from ∼N120 to 130°E in its western and eastern margins to ∼N070–090°E in its central part. Palaeomagnetic data should be useful in order to determine whether this along-strike structural variation is due to secondary rotations induced by deformation and thrust emplacement (similar to oroclinal bending) or, on the contrary, it is a primary orientation, probably linked to the structural control of basement features inherited from pre-orogenic times. In order to solve this question, 23 new palaeomagnetic sites were collected along-strike the IS, and analysed in combination with the palaeomagnetic data provided in the studies by Oliva-Urcia (2004) and Oliva-Urcia & Pueyo (2007) for the same stratigraphic units. In these previous studies, two palaeomagnetic components were reported: a poorly developed, higher-temperature component (C) which was defined in 30 per cent of the sites, and a widespread lower temperature component (B) occurring in 85 per cent of the analysed sites. The C component was interpreted as the primary magnetization because it showed normal and reverse polarities after tectonic correction and could be considered as pre-folding at regional scale (it passed McElhinny's fold test, McElhinny 1964). For the whole dataset, this component showed a better grouping after tectonic correction, although with a wide dispersion in the inclination values, ranging from subhorizontal to subvertical. The B component was always reversed in polarity and post-folding, and was interpreted as a late remagnetization which recorded a finite mean clockwise rotation of +13°.

Considering the new and previous data, this work aims to: (i) understand the remagnetization process in the Pyrenean IS and its relationship with deformation (folding and thrusting) during the Eocene orogenic stage; (ii) define the actual meaning of the higher-temperature component (C component) found in previous works and (iii) shed some light on the origin of the along-strike changes in the IS using the VARs derived from palaeomagnetic data.

2 GEOLOGICAL SETTING

The Pyrenean range is the result of the collision between the Iberian and Eurasian plates during Late Cretaceous-Miocene times. At range-scale, the Pyrenees are divided into three ESE–WNW-striking structural domains (Fig. 1a), from north to south: (i) the North Pyrenean Zone (NPZ), where thick sequences of Mesozoic rocks crop out, (ii) the Axial Zone (AZ), formed by metasedimentary and igneous rocks of Palaeozoic age and (iii) the South Pyrenean Zone (SPZ), characterized by the presence of thick syn-tectonic sequences of Cenozoic age. The Pyrenees can be described as a double-vergent, asymmetric fold-and-thrust system (Muñoz 1992; Teixell 1998; Martínez-Peña & Casas-Sainz 2003) that consists of large, south-directed thrust sheets forming the Axial and South Pyrenean Zones and a smaller retrovergent belt mainly involving the NPZ (Figs 1b and c). The present study is focused on the northern part of the South Pyrenean Zone (SPZ), in the IS domain (Fig. 1a).

2.1 Stratigraphy of the IS

The Pyrenean IS are formed by Upper Cretaceous to Lower Eocene carbonate sequences that overlie the Devonian, Carboniferous and Permian rocks that form the Western Axial Zone (Fig. 2a). The stratigraphic sequence of the IS domain includes four main units designated as: (i) Cañones limestones (Fournier 1905), (ii) Zuriza marls and limestones (Teixell 1992), (iii) Marboré sandstones (Souquet 1967) and (iv) Palaeocene–Lower Eocene carbonates (Fig. 2a, see legend):

(i) The Cañones limestones are Cenomanian to Santonian shelf carbonates with a constant thickness of ∼150 m. In the western part of the sampled area, this unit unconformably covers the Palaeozoic units of the western part of the AZ (Ríos- Aragüés *et al.* 1987a; Teixell *et al.* 1989; Teixell & García Sansegundo 1989). Towards the east, the base of the Cañones limestones unconformably overlies the Palaeozoic basement, but the upper part of the unit is affected by small-scale thrusts (Rodríguez-Méndez 2011; Rodríguez-Méndez *et al.* 2013; Ríos-Aragüés *et al.* 1987a,b).

(ii) The Zuriza Fm. consists of siliciclastic and carbonatic sediments deposited in external platform or slope environments (Teixell 1992). The unit is Campanian to Maastrichtian in age and progressively thins eastward from a maximum thickness of ∼600 m in the western edge of the AZ, grading vertically and laterally into the overlying unit, the Marboré sandstones (Teixell 1992).

(iii) The Marboré Fm. consists of middle platform bioclastic sandstones, marly limestones and marls of Maastrichtian age. They have a maximum thickness of ∼700 m to the east (Ríos-Aragüés *et al.* 1987b) that decreases towards the western part of the study area (Teixell *et al.* 1989; Teixell & García Sansegundo 1989).

(iv) The Palaeocene–Lower Eocene carbonates consists of limestones, marls and dolomites that have a constant thickness of ∼200 m throughout the study area. This unit was deposited during the last episode of platform sedimentation before the onset of turbiditic deposition in the southern Pyrenean trough.

Since the Late Santonian (i.e. after the deposition of the Cañones limestones), sedimentation was under a compressional tectonic regime, linked to the first stages of flexural bending and the early movements of the Lakora-Eaux-Chaudes thrust system (Labaume *et al.* 1985; Teixell 1992), north of the study area (see location of the Lakora-Eaux-Chaudes thrust in Fig. 1b). Convergence and syn-tectonic sedimentation continued during Cuisian to Lutetian times, with the deposition of thick sequences of turbidites (the Hecho Group, Mutti *et al.* 1972) in the Jaca-Pamplona basin (see location in Fig. 1a). The Hecho Group turbidites are alternating centimetric to decimetric beds of sandstones and shales with interbedded megaturbidites (Labaume *et al.* 1983; Mutti 1977; Barnolas & Teixell 1994; Remacha & Fernández 2003) mainly made of layers of carbonate megabreccias up to hundreds of metres thick. The turbidites lap onto the Palaeocene–Lower Eocene carbonates and have a maximum thickness of 4500 m (Teixell 1992).

2.2 Structural setting

The present-day structure of the IS is the result of superimposition of two main thrusting events (Fig. 2; Teixell 1992): (i) development of the Larra-Monte-Perdido thin-skinned thrust system and (ii) the emplacement of the Gavarnie basement nappe. The Larra-Monte-Perdido fold-and-thrust system, active during Mid-Late Lutetian to Bartonian (Remacha *et al.* 1987; Barnolas *et al.* 1991; Teixell 1992, 1996), consists of several hectometric to kilometric-scale thrust sheets involving the Upper Cretaceous and Palaeocene to Lower Eocene units of the IS, as well as the basal turbidites of the northern sector of the Jaca Basin (Figs 2b and c). The main décollement of this thrust system is located in the Zuriza Fm. (Teixell 1992), but a secondary detachment level, located in the Cañones limestones has

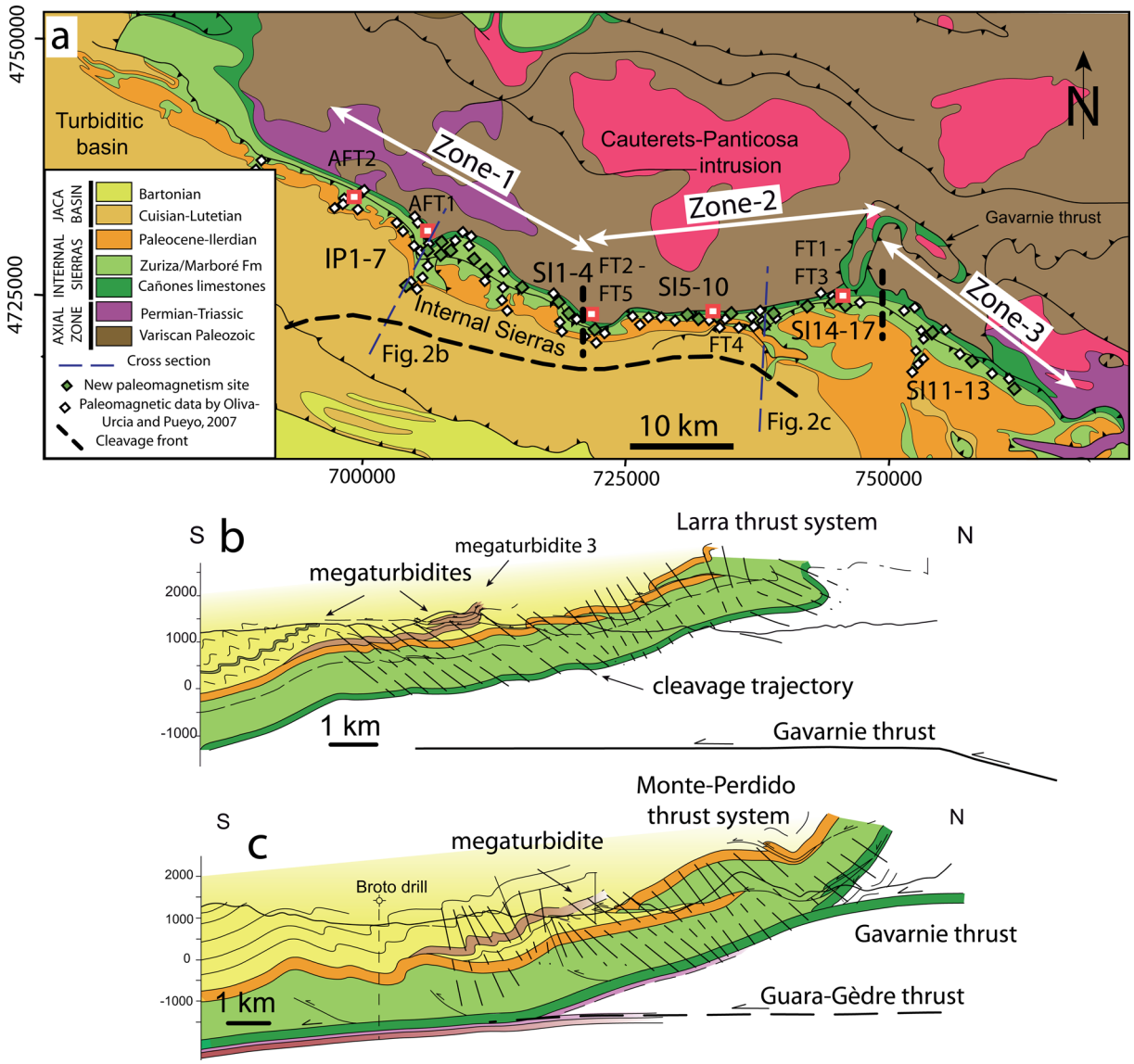

Figure 2. (a) Geological map of the study area with location of sites. Panels (b) and (c) are the geological cross sections through the western and central-eastern parts of the IS (from Izquierdo-Llavall *et al.* 2013a). Locations of the cross sections and fold structures used to carry out fold tests (FT and AFT) are also shown in Fig. 2(a) (red squares).

been reported in the central (Rodríguez-Méndez 2011) and eastern part of the study area (Ríos Aragüés *et al.* 1987b; Fig. 2c). This thin-skinned thrust system branches to the north in the Lakora-Eaux-Chaudes basement thrust (see location in Figs 1a and b).

The Larra-Monte-Perdido fold-and-thrust system was folded and deformed during Eocene–Early Oligocene due to the emplacement of the Gavarnie basement thrust sheet (Van der Voo 1966; Séguret 1972; Labaume *et al.* 1985; Teixell 1996; Millán-Garrido *et al.* 2006; Figs 2b and c). Development of this range-scale structure produced the passive folding of the basement and cover sequences in a kilometric-scale hangingwall anticline whose backlimb and forelimb crop out north and south of the AZ, respectively (Fig. 1b). The Upper Cretaceous to Eocene sequence of the IS, affected by the Larra-Monte-Perdido thrust system, was tilted southwards in the forelimb of this regional-scale structure (Figs 2b and c). The Gavarnie thrust is folded by underlying basement thrusts (Bielsa, Fig. 1c, and Guara-Gèdre, Fig. 2c, Millán-Garrido *et al.* 2006) that are limited to the eastern part of the IS and transported southwards by the Guarga thrust sheet (see Figs 1b and c).

The Gavarnie thrust has been interpreted to be linked to a cleavage-related folding event (Labaume *et al.* 1985; Teixell 1992; Izquierdo-Llavall *et al.* 2013a; Rodríguez *et al.* 2014) that affected the whole stratigraphic sequence (from the Palaeozoic basement in the AZ up to the top of the turbidites of the Hecho Group; Fig. 2 and 3). The chronological relationship between cleavage-related folding and the southwards tilting of the IS in the forelimb of the Gavarnie hangingwall anticline (Teixell 1992; Rodríguez-Méndez 2011; Izquierdo-Llavall *et al.* 2013b; Muñoz *et al.* 2013 and references therein) indicates a diachronous development of regional cleavage with layer-parallel shortening predating folding and cleavage-related folds developed prior or coevally to the southwards rotation of bedding. The cleavage front (surface separating cleaved from uncleaved units) is oblique to the general trend of folds and its position has been interpreted to be thermally controlled

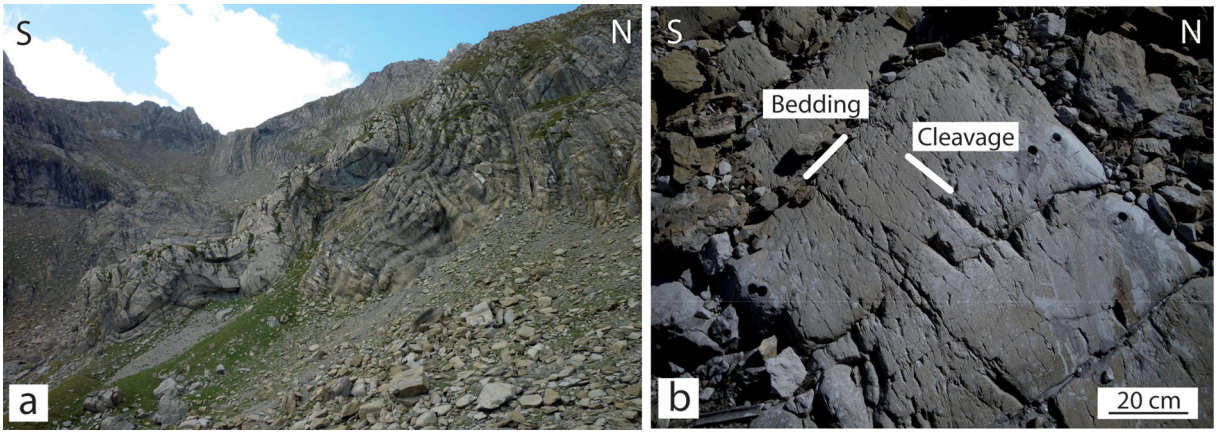

Figure 3. (a) Cleavage-related folds deforming the Zuriza Fm. (b) North-dipping cleavage surfaces affecting south-dipping bedding planes.

(Holl & Anastasio 1995; Izquierdo-Llavall *et al.* 2013a). In the IS, vitrinite reflectance data indicate that cleavage developed at peak temperatures ranging between 160 and 190 °C (Izquierdo-Llavall *et al.* 2013a; Fig. 3b).

3 METHODOLOGY

3.1 Sampling sites

Twenty-three new palaeomagnetic sites, distributed ∼50 km along the strike of the IS, were sampled with a portable water-cooled drill. Each site consists of 9–12 cores distributed through about 10–20 m of the stratigraphic succession. In each site, bedding and cleavage orientations were measured (Fig. 3b). Two main considerations were taken into account during the sampling work:

(i) Samples were collected from the portion of the stratigraphic sequence below the main detachment level of the Larra-Monte-Perdido fold-and-thrust system. These sites can be assumed to only register VARs related to basement kinematics (additional VARs related to thin-skinned tectonics could occur in the upper portion of the sedimentary sequence of the IS).

(ii) The samples were collected from the Marboré (19 sites) and the Zuriza (4 sites) Fms because the study by Oliva-Urcia & Pueyo (2007) showed that these two units exhibit a more stable palaeomagnetic behaviour at high temperature than the Cañones limestones. Fine-grained, marly beds were preferably sampled and therefore, although samples belong to two different formations, they are lithologically similar. Additionally, we sampled particular sites for conglomerate and fold tests to better constrain the age of magnetization. One site (IP7) was sampled in one of the northern megaturbidites interbedded in the turbiditic infill of the Jaca-Pamplona basin (the megaturbidite 3 or Villanúa megaturbidite, see location in Fig. 2b). This megaturbidite is ∼200 m thick (Teixell *et al.* 1989) and its base is made of a carbonate megabreccia containing clasts of centimetric to hectometric size eroded from the Palaeocene–Lower Eocene carbonates and the Zuriza marls. This basal megabreccia was sampled for a conglomerate test. Besides, two hectometric-scale folds were sampled in the central part of the study area (sites SI8 and SI10 and sites SI16 and SI17) for fold tests.

3.2 Laboratory procedures

3.2.1 Demagnetization of the samples

Specimens were measured and demagnetized at the Pacific Northwest Palaeomagnetic Laboratory (Western Washington University, WA, USA) in a magnetically shielded room. Two samples per site were selected for pilot thermal and AF demagnetizations, using an ASC oven (Model TD48) and a D-Tech D-2000 AF demagnetizer, respectively. Magnetizations were measured with a 2-G cryogenic magnetometer and susceptibility was monitored during thermal demagnetization using a Bartington MS-2 dual frequency susceptibility meter. In the thermal demagnetizations, most of the pilot samples showed a sharp increase in susceptibility and magnetic moment at temperatures between 450 and 550 °C that was accompanied by strong changes in the direction of the magnetization. AF demagnetization was effective (the remanent magnetization at 100–125 mT is lower than 20 per cent of the NRM) in 78 per cent of the pilot samples but complex demagnetization diagrams were obtained in ∼40 per cent of the specimens.

To evaluate the influence of coarse grain magnetite, additional samples underwent a low temperature treatment (Housen *et al.* 2003): they were submerged in liquid nitrogen (∼77 K) for 10–15 min, warmed at low magnetic field in the air-cooled end of the TD48, and their magnetization was measured immediately after warming them to room temperature. Significant differences in magnetizations were observed between the NRM and the measurements after the low-temperature treatment, evidencing the contribution of coarse grain magnetite (which usually carries viscous, recent magnetizations without interest from the geological point of view) to the natural remanent magnetization of the samples.

Considering the results of the pilot experiments, we decided to adopt the following demagnetization procedure: (1) measurement of the NRM, (2) low temperature treatment of the samples to eliminate the contribution of coarse grain magnetite, (3) thermal demagnetization up to 400 °C and (4) AF demagnetization to fully remove the remaining magnetization. The palaeomagnetic components were fitted using the PCA method (Kirschvink 1980) and site means and confidence angles were computed using Fisher (1953) statistics. For both, we used the software Remasoft (Chadima & Hrouda 2006). The statistical confidence of the fold test was determined by McFadden & Jones (1981) method.

In site IP7 (conglomerate test), 10 samples from different carbonate and marly clasts and nine samples from the fine-grained carbonate matrix were demagnetized (note the lithological similarity between the clasts and the matrix). The results of this conglomerate test are key data in the understanding of the acquisition time for the palaeomagnetic components in the IS.

3.2.2 Magnetic mineralogy analyses

Different magnetic mineralogy experiments were conducted on the samples from the Marboré and the Zuriza Fms. in order to characterize the carriers of the palaeomagnetic components. The rock magnetism analyses comprise (i) isothermal remanent magnetization (IRM) acquisition curves (Dunlop 1972) and backfield experiments, (ii) thermal demagnetization of composite IRM (Lowrie test; Lowrie 1990) and (iii) hysteresis loops. All the experiments were performed in the Pacific Northwest Palaeomagnetic Laboratory (Western Washington University, USA).

IRM acquisition curves, backfield experiments and hysteresis curves were measured on 24 rock chips (0.3–0.5 g) using a Vibrating Sample Magnetometer (Princeton Measurements Corporation, MicroMag model 3900). IRM and backfield curves were defined by 25 measurements of magnetic remanence in non-linearly increasing magnetic fields up to a maximum of 1 T. Additional measurements of IRM acquisition up to 2.5 T were conducted on 12 selected standard specimens using a pulse magnetizer (ASC Scientific, Model IM-10–30). Hysteresis measurements on the same chips were averaged over five field cycles up to 1.5 T.

Stepwise thermal demagnetization of composite IRM was performed in one standard specimen per site. The IRM was imparted in three decreasing magnetic fields (2.5, 0.12 and 0.02 T) along $+Z$, $+Y$ and $+X$ axes, respectively, prior to thermal demagnetization. The magnetic fields were applied using a pulse magnetizer (ASC Scientific, Model IM-10–30) and their intensities were selected considering AF demagnetization behaviours as well as the samples response to the low-temperature treatment.

4 STRUCTURAL DATA

In map view, the IS display an arcuate geometry due to along-strike changes in the trend of the structure. Three different zones can be recognized at regional scale (see location in Fig. 2a): zone 1, to the west, with N120ºE trend; zone 2, in the central part of the study area, with N080ºE trend and zone 3, to the east, with N125ºE trend. This change in the general trend of the structure is also recognized in the distribution of bedding and cleavage planes (Fig. 4). Rose diagrams constructed from structural data collected in different transects indicate dominant bedding strikes that range between N100°E and N120°E in zone 1 (western part), between N070°E and N090°E in zone 2 (central part) and between N100°E and N140°E in zone 3 (eastern part). The strike of cleavage approximately mimics the distribution of bedding strikes: cleavage is N090–N120°E-striking in zone 1, N070°E–N100°E-striking in zone 2 and N110–N120°E-striking in zone 3. Most bedding planes dip shallowly to the south, but shallowly north-dipping or intermediate to steeply south-dipping planes are recognized in zones 1 and 2, respectively (Fig. 4).

Cleavage has shallow to steep dips to the north, except in particular outcrops located in zone 2, where cleavage dips south (Fig. 4). The intersection lineation between cleavage and bedding is typically subhorizontal and with trend that changes along-strike as the strike observed in both cleavage and bedding planes (Fig. 5).

5 PALAEOMAGNETIC DATA

5.1 Magnetic mineralogy of the Marboré and Zuriza units

The analysed samples had NRM moments ranging between 3.6 and 0.04 mA/m and magnetic susceptibilities between 40 and 209 $\times$ 10^{-6} SI (average of 124 $\times$ 10^{-6} S.I. units, Table 1). Samples from most sites in the Marboré and Zuriza Fms have similar magnetic behaviours as documented by the IRM and composite IRM analysis.

IRM acquisition curves show that most (~75 per cent) of the selected samples are totally (or almost totally) saturated at magnetic fields that vary between 150 and 900 mT but are generally below 500 mT (Fig. 6a). The coercivity of remanence in the backfield analysis (Hcr) ranges between ~15 and 55 mT. In 25 per cent of the analysed samples (from sites SI1, SI3, SI6, SI7, SI9, SI13 and SI14), IRM acquisition curves do not reach saturation and have values of Hcr (ranging between 35 and 1200 mT) that would indicate varied contributions of low and high-coercivity carriers (Fig. 6b). The separation of components by means of the IRM-CLG 1.0 worksheet (Kruiver *et al.* 2001) distinguishes three different ferromagnetic contributions (Figs 6c and d):

(1) A low coercivity component (component 1 in Fig. 6c) that was defined in ~30 per cent of the samples, has a mean coercivity ($B_{1/2}$) between 5 and 25 mT and contributes 10–35 per cent to the total IRM.

(2) An intermediate coercivity component, found in all the analysed samples (component 2 in Figs 6c and d), that has a mean coercivity ($B_{1/2}$) ranging between 30 and 40 mT and contributes 10–100 per cent to the total IRM. In all non-saturated curves, the contribution of this component is lower than 65 per cent.

(3) A hard magnetic carrier which contributes 5–90 per cent to the IRM and occurs in ~50 per cent of the samples (component 3 in Fig. 6d). Non-saturated curves show the highest contributions (>35 per cent) of this hard magnetic component.

Results of stepwise thermal demagnetization of composite IRM (Lowrie test; Lowrie 1990; Fig. 7) indicate that, in 65 per cent of the analysed samples, most of the magnetization is along the intermediate axis (120 mT) and shows a sharp decay at temperatures of 500–575 °C, in the range of magnetite (Fig. 7a). In 35 per cent of the samples, curves indicate the dominance of a hard coercivity carrier (hard axis, 2.5 T) that unblocks between 660 and 690 °C, in the range typical of haematite (Fig. 7b), although the hard axis commonly shows an additional intensity decay at around 325 °C that indicates the presence of iron sulphides, probably pyrrhotite (Fig. 7a). Most of the composite IRM diagrams show that a small part of the magnetization is along the soft axis (20 mT) and probably corresponds to the coarse grain magnetite (MD magnetite) whose contribution was inferred from the low temperature treatment results. The relative contribution and coercivities of the three components isolated in the composite IRM are consistent with those defined from the IRM acquisition curves: the soft (MD magnetite), intermediate (SD magnetite) and hard axis (iron sulphides and haematite) in the composite IRM correspond to the low, intermediate and high coercivity components inferred from the IRM decomposition.

Although the presence of high coercivity minerals is detected by the IRM and composite IRM analysis, it is important to note

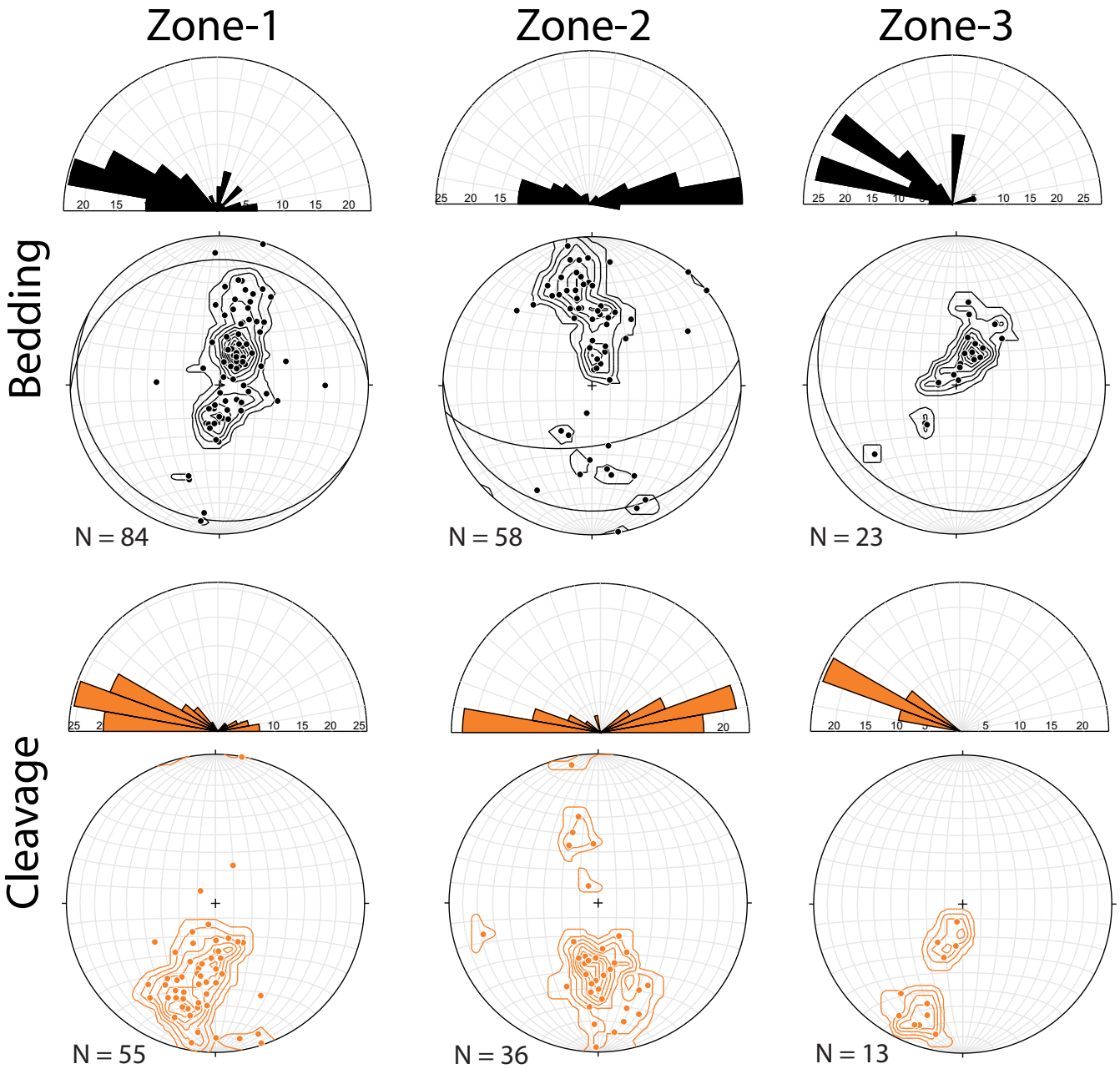

Figure 4. Equal area plots and rose diagrams showing the orientation of cleavage and bedding planes in the three along-strike sectors recognized in the IS. Rose diagrams show the dominant strike for bedding and cleavage planes. Plots show the orientation of the poles to bedding and cleavage planes and the corresponding density diagrams (contour interval = 2–5 per cent). Great circles represent bedding planes corresponding to pole maxima and sub-maxima in the density diagrams. Plots were generated using the Stereonet 8.8.6 program (Allmendinger *et al.* 2013; Cardozo & Allmendinger 2013).

that (i) remanence was cancelled in almost 80 per cent of the AF pilot samples, (ii) the combined thermal (up to 400 °C) plus alternating field demagnetization was successful in 27 out of the 28 sites and (iii) unblocking temperatures are generally in the range of magnetite. These results indicate that although hard or intermediate magnetic carriers (iron sulphides and haematite) are present in the analysed samples they do not significantly contribute to the remanent magnetization.

Hysteresis loops usually show a wasp-waisted shape (Fig. 8), typical of remagnetized carbonates (Jackson 1990; Channell & McCabe 1994) with SD and SP (single domain and superparamagnetic) magnetite mixtures (Tauxe *et al.* 1996) or with different ferromagnetic phases (Muttoni 1995; Roberts *et al.* 1995). In site SI-6 (Fig. 8d), where hard magnetic minerals were detected (Figs 6b and d), the hysteresis loop shows a goose-necked shape, typical of magnetite and haematite mixtures (Tauxe 2008). The Day diagram (Fig. 9, Day *et al.* 1977) was constructed from the parameters obtained in the hysteresis loops and the back-field experiments. The distribution of the samples in the Day plot indicates a mixture of single domain (SD) and multidomain (MD) grains with the location of the samples between the SD + MD and the SP + SD theoretical mixing curves (Dunlop 2002).

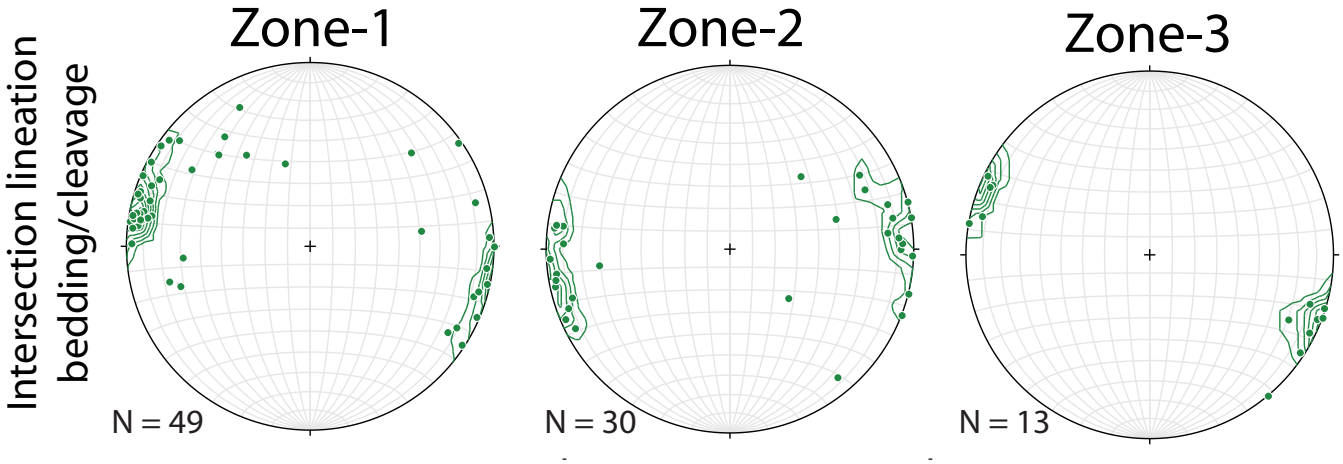

Figure 5. Equal area plots and density diagrams (contour interval = 2 per cent) showing the orientation of the intersection lineation between cleavage and bedding planes for the three zones distinguished in the IS.

Table 1. New palaeomagnetic sites sampled in the Upper Cretaceous units of the IS. Name of the site (for location in map view see Fig. 2a); stratigraphic unit (MS, Marboré sandstones; ZM, Zuriza marls; MG3, megaturbidite 3 or Villanúa megaturbidite); location in UTM coordinates (ED50 datum 30 T zone); along-strike location of the site; site mean Natural Remanent Magnetization (NRM) intensity (in mA/m) and bulk magnetic susceptibility (km) (10^{-6} S.I.). Site IP7 was used for a conglomerate test; matrix and clasts were sampled.

Site	Stratigraphic unit	UTM *x* (Easting)	UTM *y* (Northing)	Sector	Mean NRM intensity (mA m^{-1})	Mean km (10^{-6} S.I.)
IP-1	MS	706866	4733984	zone-1	0.521	137
IP-2	ZM	707675	4733340	zone-1	0.729	200
IP-3	ZM	705493	4734132	zone-1	0.199	97
IP-4	ZM	703928	4734825	zone-1	0.114	110
IP-5	ZM	704834	4734097	zone-1	0.773	162
IP-6	MS	702895	4733468	zone-1	0.512	179
IP-7	MG 3-matrix	702379	4729331	zone-1	1.07	138
IP-7	MG 3-clasts	702379	4729331	zone-1	1.68	222
SI-1	MS	716036	4729741	zone-1	0.88	81
SI-2	MS	716469	4730002	zone-1	0.0575	61
SI-3	MS	717010	4729034	zone-1	0.613	115
SI-4	MS	719547	4726607	zone-2	0.553	122
SI-5	MS	735868	4729123	zone-2	0.0772	100
SI-6	MS	736887	4730189	zone-2	1.78	148
SI-7	MS	733225	4729929	zone-2	0.0404	85
SI-8	MS	730246	4729687	zone-2	3.60	90
SI-9	MS	730926	4729521	zone-2	2.17	116
SI-10	MS	732093	4729446	zone-2	2.64	134
SI-11	MS	755960	4726859	zone-3	0.525	64
SI-12	MS	761740	4723354	zone-3	0.389	134
SI-13	MS	753615	4727849	zone-3	0.237	40
SI-14	MS	740547	4731460	zone-2	0.0911	67
SI-16	MS	743319	4731449	zone-2	0.731	169
SI-17	MS	742816	4731683	zone-2	0.817	209

5.2 New palaeomagnetic data

Stepwise thermal and AF demagnetizations reveal the presence of two stable palaeomagnetic components: a lower temperature component (component B, in Table 2) and a higher temperature component (component C, in Table 3) that occur together in ∼50 per cent of sites. Furthermore, there is an additional low temperature, viscous component (component A in Fig. 10) that unblocks between 100 and 200 °C and occurs in almost 75 per cent of the demagnetized samples. This component has a mean orientation (Dec = 357°, Inc = 65°) that corresponds to the present-day magnetic field although it shows a substantial dispersion. The B component unblocks between 200 °C and 325–400 °C (Figs 10a, b and f) during thermal demagnetization, or under low magnetic fields (15 to 25–35 mT) if it is well isolated in AF demagnetization. This component occurs in 12 of the 23 sites and is especially well-developed in the sites from the western part of the study area. Component C has been defined in 70 per cent of the sites. In samples that remained stable during high-temperature demagnetization steps, we observe that this component shows maximum unblocking temperatures of 500–575 °C (Fig. 10e; except in samples from site SI6, where the maximum unblocking temperature is 670–690 °C, Fig. 10d). Nonetheless, in

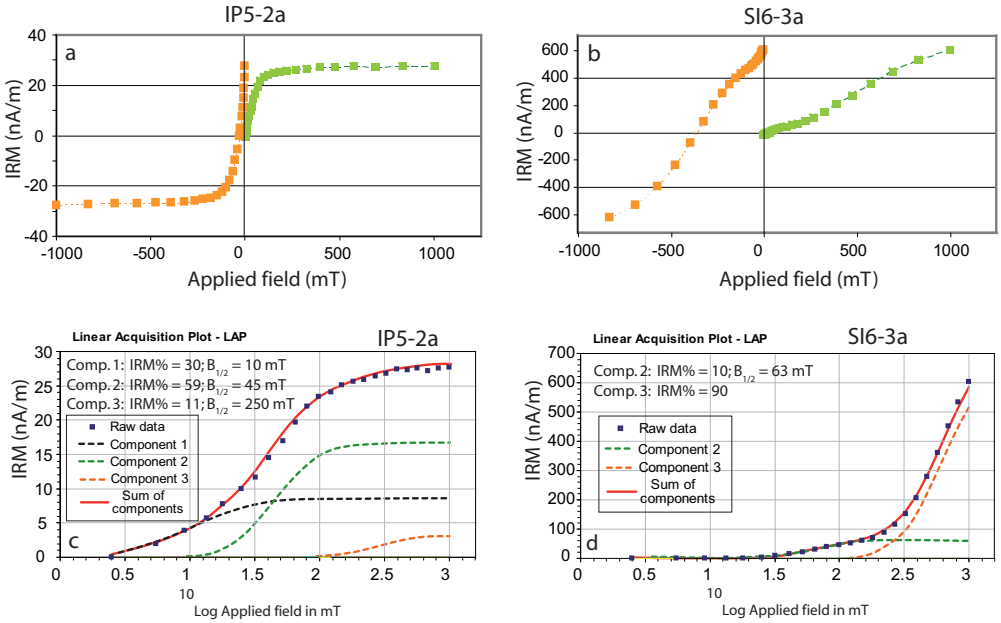

Figure 6. IRM acquisition curves (green colour) and backfield experiments (orange colour) in two samples from sites IP5 (Zuriza marls) and SI6 (Marboré sandstones). The sample from site SI6 is not saturated in an applied field of 1 T. The IRM acquisition curves shown were obtained using a Vibrating Sample Magnetometer (a–b). IRM acquisition curves to higher fields required use of a pulse magnetizer, with remanence measured on the magnetometer. Decomposition of the curves utilized the IRM-CLG 1.0 worksheet (Kruiver *et al.* 2001; c–d).

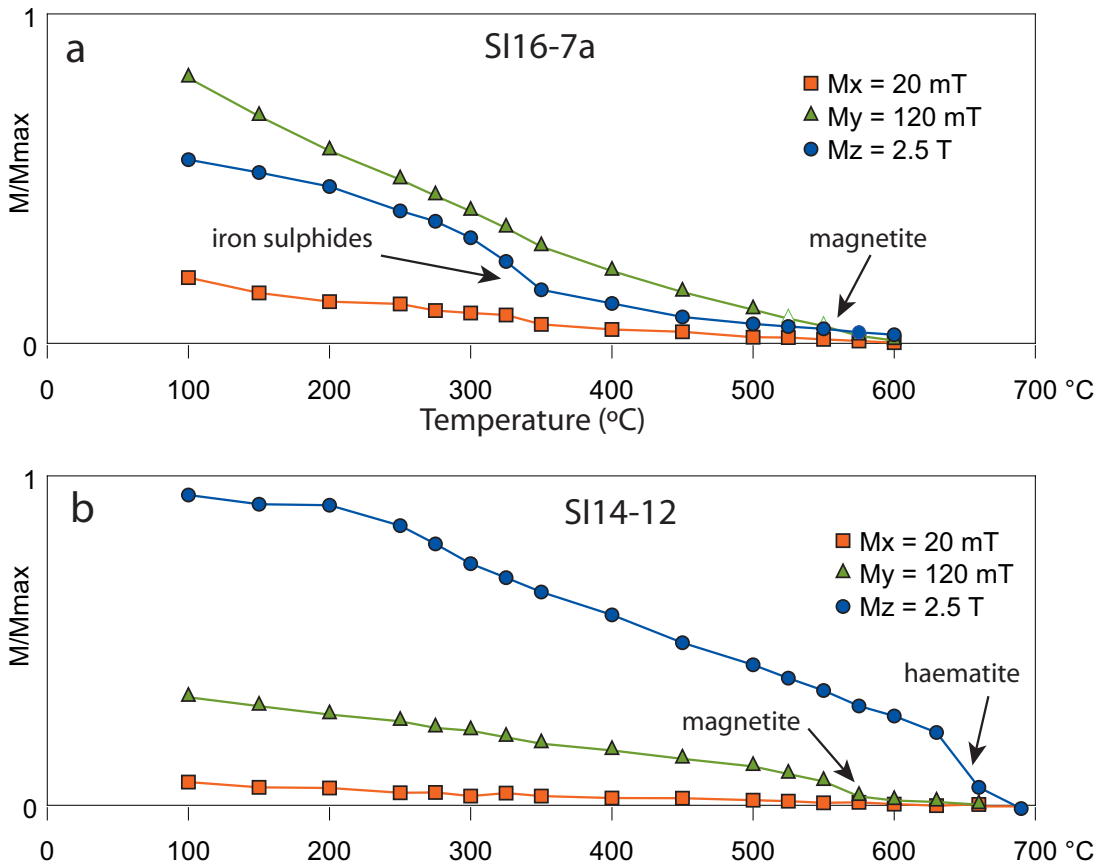

Figure 7. Intensity decay of the stepwise thermal demagnetization of composite IRM in samples from sites SI16 and SI14 (Marboré sandstones). Mz, My and Mx is the magnetic moment along $+Z$, $+Y$ and $+X$ axes acquired in 2.5, 0.12 and 0.02 T fields, respectively. *Y*-axis, normalized remanent magnetization; *X*-axis, temperature.

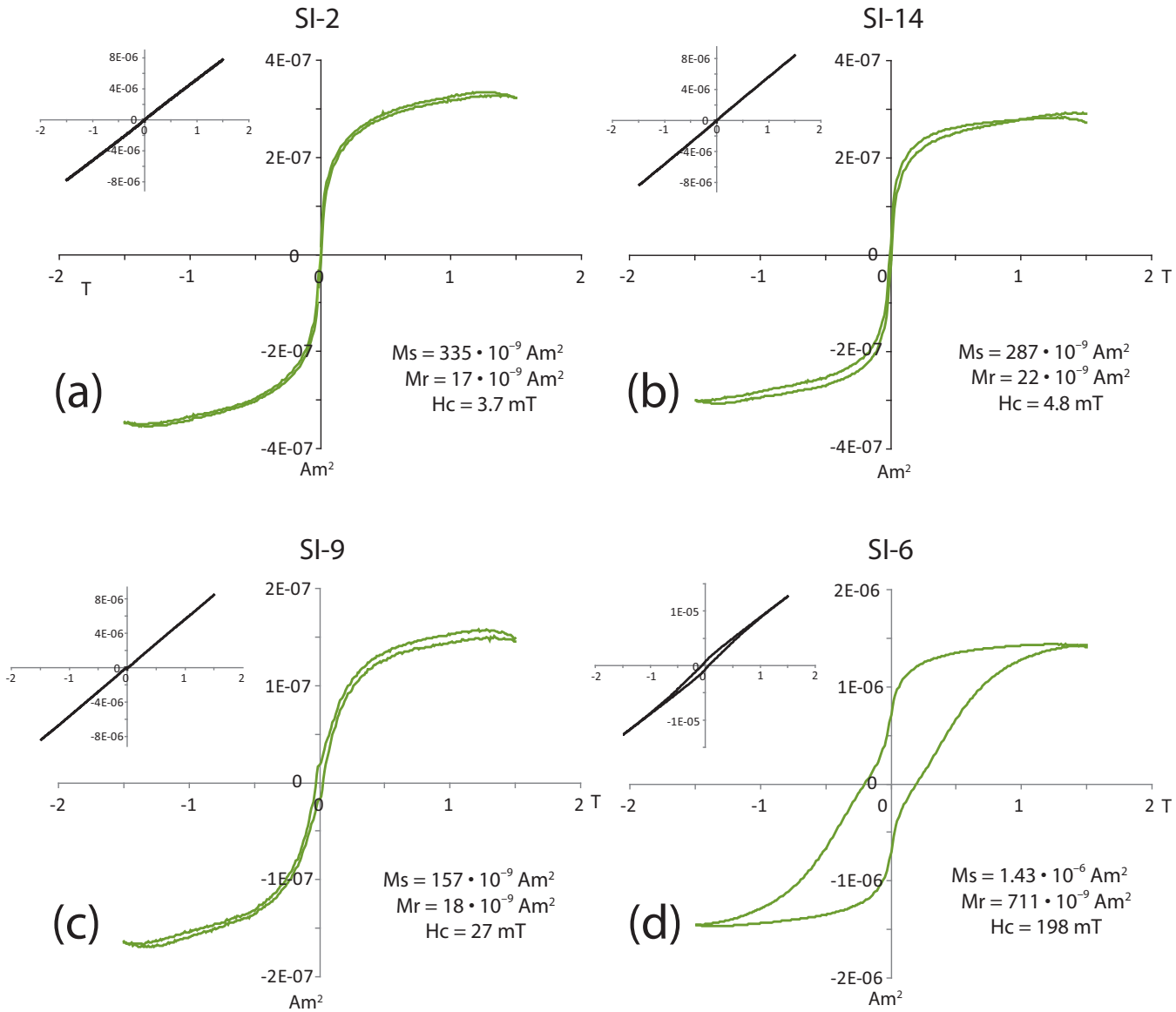

Figure 8. Slope corrected hysteresis loops from chips. The positive slope in the smaller diagrams of uncorrected hysteresis loops indicates a strong paramagnetic contribution.

most of the samples, component C has been mainly isolated with AF demagnetization to 50–100 mT after heating the sample up to 400 °C (Figs 10a, b and f). The observed unblocking temperatures and AF effective fields are consistent with the magnetic mineralogy experiments and evidence that magnetite is the main carrier of both, components B and C (although a small contribution of pyrrhotite cannot be completely discarded as carrier of the B component). Only in site SI-6 was a higher unblocking temperature (∼670–690 °C) detected (Fig. 10d), which indicates that the C component is carried by haematite (component B is not present). According to polarity and unblocking temperatures, the described B and C components correspond to the B and C components, respectively, defined by Oliva-Urcia & Pueyo (2007) in this area.

The B component is better grouped in geographic coordinates (Dec = 192°, Inc = 45°, α_{95} = 9°, k = 22, N = 12 sites) and has a constant reverse polarity (Fig. 11a). After tectonic correction, component B has a higher dispersion, with directions distributed along a N–S great circle that is perpendicular to the regional fold axes (Fig. 11b). This distribution strongly suggests a post-folding acquisition of component B, which is confirmed by the two fold tests (FT1 and FT2; the latter in Fig. 11c) presented in Table 4.

Component C shows a bimodal distribution but dominant normal polarities in geographic coordinates (Fig. 12a). After bedding correction, 60 per cent of the sites show normal polarities with variable inclinations (ranging between 25 and 70°) and 20 per cent of the sites display a reverse polarity (Fig. 12b). Three fold tests were carried out in folds of hectometric to kilometric wavelength, located in the central and western part of the study area (zones 1 and 2, see location in Fig. 2a). A complex timing of remagnetization relative to folding that varied along strike is inferred for component C (Table 4) because:

(i) To the eastern part of zone 2 (sampling sites SI16–SI17, Fig. 2a), the fold test is positive at the 95 per cent level of confidence and indicates a pre-folding acquisition of component C, that is reversed in polarity after bedding correction (FT3 in Table 4, Fig. 12c).

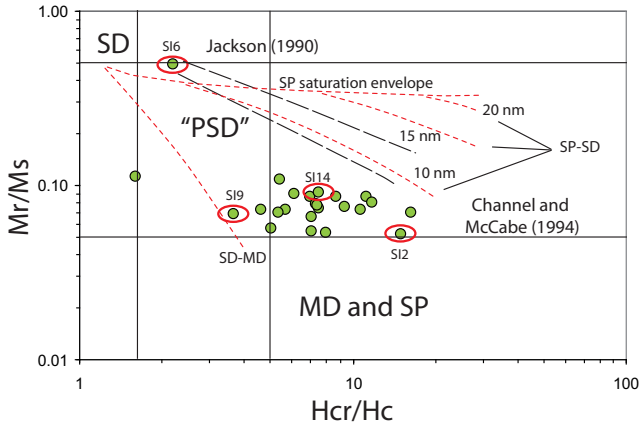

Figure 9. Day diagram for samples from the Internal Sierras (Zuriza and Marboré Fms.). The samples shown in Fig. 8 are marked. Data are compared to theoretical mixing curves (red lines) by Dunlop (2002) and to curves obtained from natural remagnetized carbonates (black lines, Jackson 1990; Channell & McCabe 1994). Our samples lay along strike between the SD + MD and SP + SD model curves (i.e. have similar Mr/Ms but varying Hcr/Hc).

(ii) In the central part of zone 2 (sites SI8–SI10), component C has almost antipodal directions in geographic coordinates and a relatively better grouping in geographic coordinates than after tectonic correction (if site SI-8 is inverted, see Fig. 12d). These results suggest that the time of acquisition of the C component varied from the northern to the southern limb of the sampled structure, and points to a late syn-folding to post-folding acquisition during a certain time window (at least two different chrons with different polarity). The fold test is significant at the 95 per cent level of confidence and indicates a late synfolding acquisition for component C, with the best statistical solution for 20 per cent of unfolding (FT4 in Table 4; Fig. 12d). The orientation of the C component for the optimal unfolding (Dec = 166°, Inc = 45°) is not consistent with the expected palaeofield direction for the study area during Cretaceous–Cenozoic times (see comments in Section 5.3), and this anomalous orientation suggests later reorientation during a post-folding tectonic event.

(iii) in the transition between zones 1 and 2 (sites SI-3 and SI-4), the fold test is significant at the 95 per cent level of confidence and shows a syn-folding acquisition for component C, with the best statistical solution for the 60 per cent of unfolding (FT5 in Table 4; Fig. 12e). The orientation of the C component for the optimal unfolding percentage is Dec = 359°, Inc = 41°.

Table 2. Palaeomagnetic data for component B. *n*/*N*, number of samples used to calculate the mean from the total number of standard samples; *D* and *I* (BTC), declination and inclination before tectonic correction; α_{95} and *k*, statistical parameters for a Fisherian distribution; So-strike, So-dip, bedding plane (strike and dip); *D* and *I* (ATC), declination and inclination after tectonic correction.

Site	*n*/*N*	*D* (BTC)	*I* (BTC)	α_{95}	*k*	So-strike	So-dip	*D* (ATC)	*I* (ATC)
IP-1	8/9	210	−47	10	33	120	41S	223	−88
IP-2	7/9	195	−44	7	78	110	37S	177	−80
IP-3	8/9	190	−31	10	34	115	25S	182	−55
IP-4	7/9	197	−34	10	41	110	46S	187	−80
IP-5	8/9	188	−22	10	33	10	26NW	179	−19
IP-6	7/9	180	−26	11	34	0	13W	174	−25
IP-7	15/18	194	−50	9	20	94	39S	268	−84
SI-1	5/9	191	−54	14	29	105	56S	28	−79
SI-2	5/9	217	−41	21	14	123	27S	221	−67
SI-4	5/9	187	−58	10	59	98	73S	8	−49
SI-16	7/9	183	−70	14	19	86	21S	305	−88
SI-17	7/9	173	−56	11	33	66	56S	313	−65

Table 3. Palaeomagnetic data for component C (key as in Table 2). (o) Overturned bedding plane. Last three lines are the data from Oliva-Urcia & Pueyo (2007) that were used in the additional fold tests.

Site	*n*/*N*	*D* (BTC)	*I* (BTC)	α_{95}	*k*	So-strike	So-dip	*D* (ATC)	*I* (ATC)
IP-1	8/9	5	35	11	27	120	41S	327	67
IP-2	8/9	9	30	9	41	110	37S	355	66
IP-3	9/9	14	29	5	108	115	25S	8	53
IP-4	7/9	25	15	6	103	110	46S	30	60
IP-5	9/9	20	25	8	42	10	26NW	7	27
IP-6	7/9	16	36	10	39	0	13W	6	38
IP-7	18/18	353	31	6	35	94	39S	337	69
SI-1	4/9	184	−3	18	27	105	56S	177	−49
SI-3	8/9	358	21	8	49	109	36S	345	53
SI-4	7/9	8	−2	13	22	98	73S	7	71
SI-6	6/9	184	−36	11	39	102	15N	185	−21
SI-8	6/9	355	−20	16	18	84/91	41/70N(o)	196	81
SI-10	6/9	154	54	12	32	90	42S	164	14
SI-13	3/9	20	49	24	26	0	0	20	49
SI-16	8/9	189	−17	14	16	86	21S	192	−38
SI-17	8/9	190	22	17	12	66	56S	191	−25
TOR-2	17/25	18	22	5	41	110	22N(o)	198	0
MG-2	10/10	189	18	10	25	114	60S	185	−40
ARG-4	8/12	23	34	9	63	40	12N	16	30

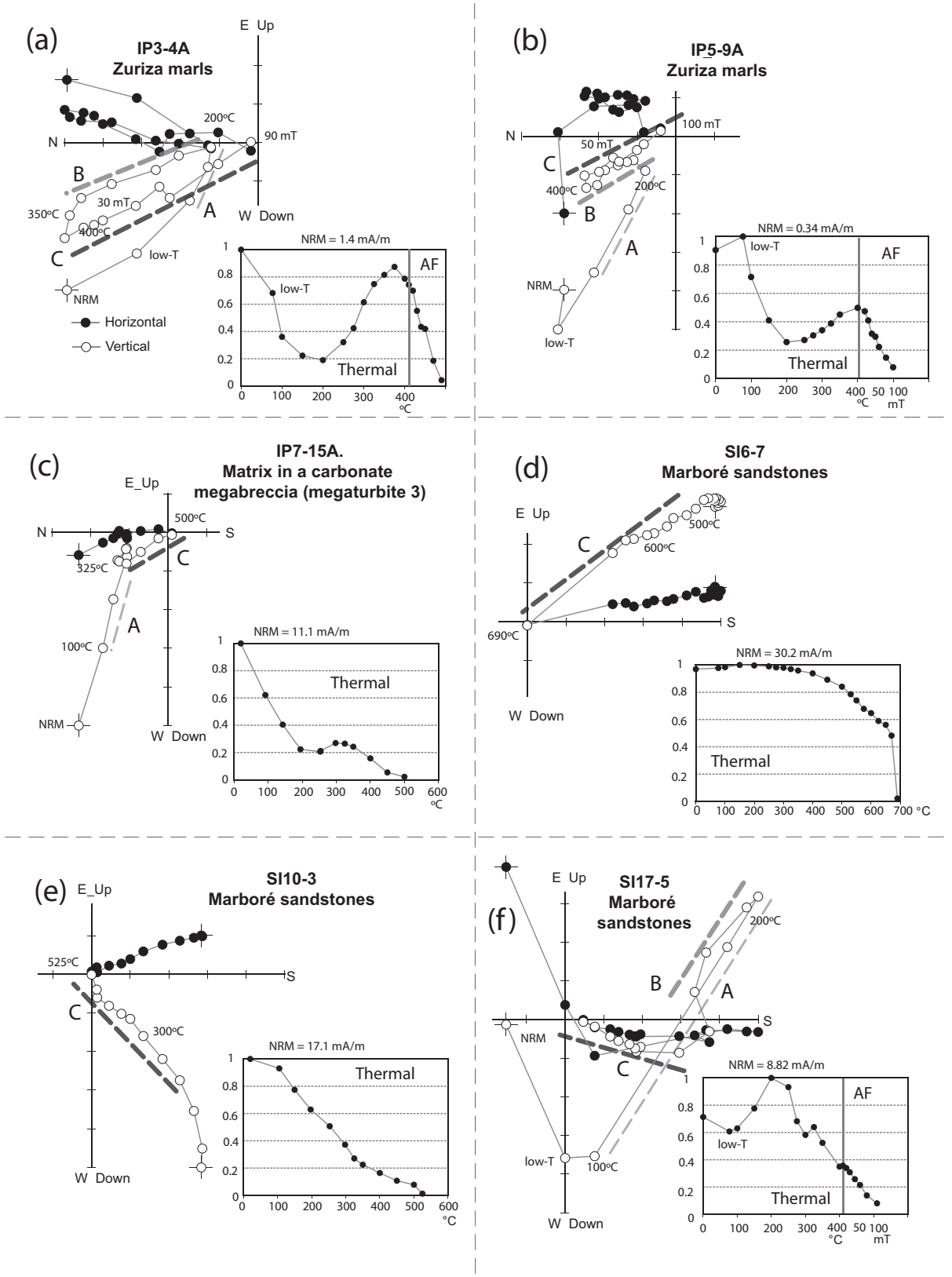

Figure 10. Palaeomagnetic results from the stepwise thermal and alternating field demagnetization shown in orthogonal diagrams in geographic coordinates and normalized intensity plots. In the orthogonal diagrams, black (white) circles are projected on the horizontal (vertical) plane. Segments interpreted as A, B and C components are highlighted in grey and black dashed lines, respectively.

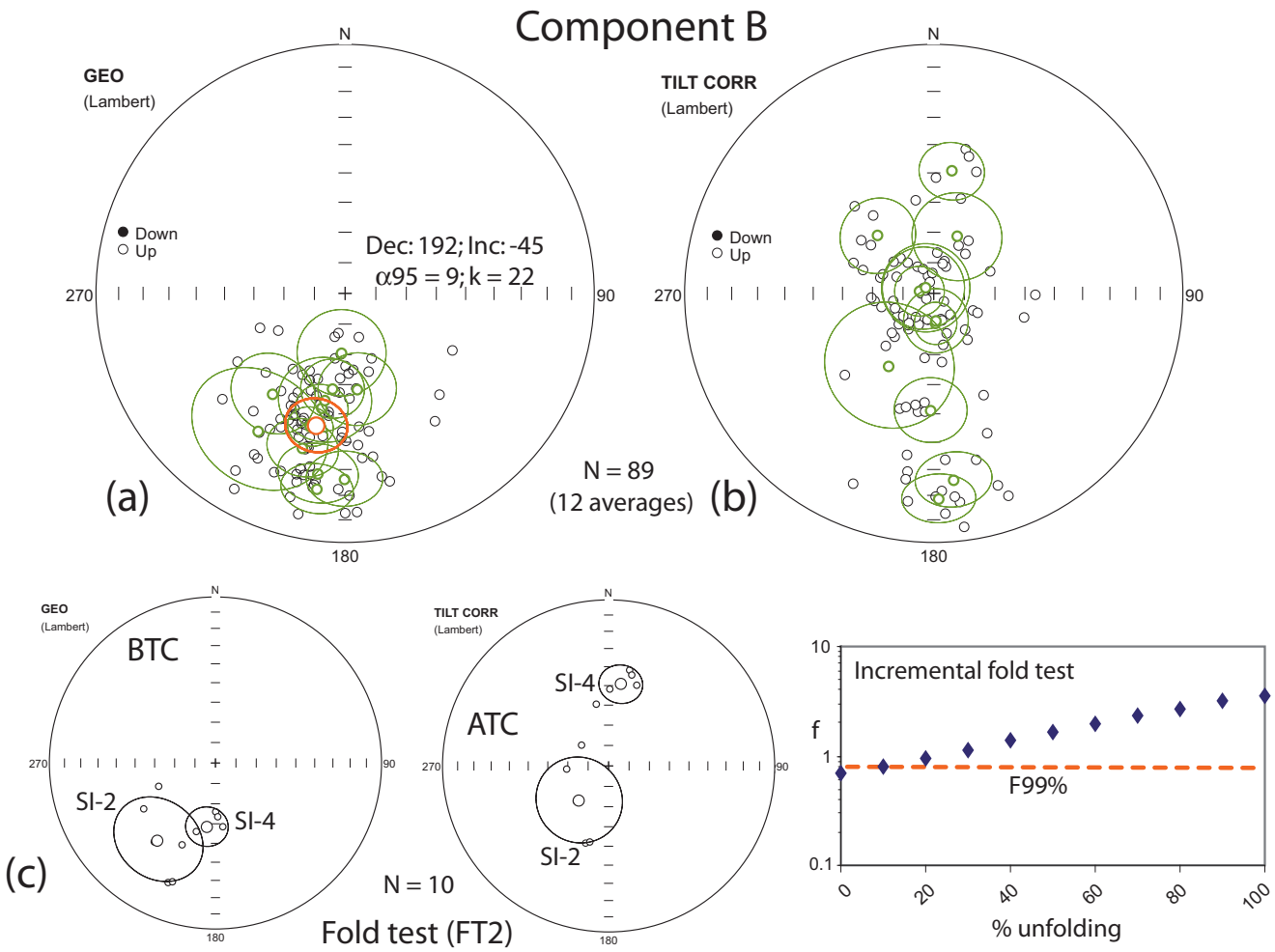

Figure 11. Equal area plots showing components B and C for the whole dataset of new palaeomagnetic sites (a) in geographic coordinates (BTC) and (b) after tectonic correction (ATC). Black, green and orange data are specimen, site mean and total mean palaeomagnetic components. (c) Graphical and incremental fold tests (FT2) for component B. The incremental fold test shows the variation of the *f* parameter in logarithmic scale (fold test statistical parameter, McFadden & Jones 1981) during progressive unfolding. The *f* parameter is compared to the value of F99 per cent (99 per cent significance level of *f*). The optimal unfolding corresponds to the minimal values of *f*. Statistics for the fold test are in Table 4.

Towards the western part of the study area (zone 1), folds could not be sampled in this work. Nonetheless, data from Oliva-Urcia & Pueyo (2007) allow the elaboration of the two additional fold tests in Fig. 13:

(i) For the Aragón valley (zone 1, sites TOR2, from Oliva-Urcia & Pueyo 2007, and IP4, from this study, see Table 3), the fold test shows the optimal grouping of the C component for −10 to −1 per cent of unfolding (post-folding acquisition). In the discussion we will refer to this fold test as AFT1 (additional fold test 1).

(ii) Conversely, for the Lizara valley (zone 1, sites MG2 and ARG4, from Oliva-Urcia & Pueyo 2007), the fold test shows the optimal grouping of the C components for 82–106 per cent of unfolding (pre-folding acquisition). In the discussion we will refer to this fold test as AFT2 (additional fold test 2).

From the fold-test results, a complex relationship between the acquisition time of component C and the progression of folding is inferred. A discussion in terms of different folding or thrusting stages and/or acquisition times will be addressed in Section 6.2.

The conglomerate test results in site IP7 (where beds dip shallowly to the south) are a significant clue in understanding the palaeomagnetic data in the IS. Both the B (with reverse polarity) and the C (with normal polarity) components can be clearly identified in both matrix and clast samples. Directions from clasts and matrix overlap (Fig. 14) and are well grouped. These results indicate that both components have a secondary origin (i.e. result from post-depositional remagnetization).

5.3 Palaeomagnetic references

To quantify the amount of vertical and horizontal axis rotations it is necessary to compare our dataset to a reference direction in the study area during the time of acquisition of the magnetization. The conglomerate test results (see Section 5.2) indicate that the observed palaeomagnetic components are not primary: we are not detecting a characteristic remanent magnetization acquired during deposition of the Marboré and Zuriza Fms. (Campanian to Maastrichtian age). On the contrary, both palaeomagnetic components correspond to remagnetizations at different stages during Pyrenean folding in this

Table 4. Fold test results. Structure where the fold test was applied, sites considered for the test, name of the component, number of samples. Declination, Inclination and the corresponding fisherian parameters (α_{95} and k) for the average, *in situ* and after bedding correction. *f*: McFadden & Jones (1981) fold test statistical parameter; *F*: 95 and 99 per cent significance level value of *f*. The last column is the fold test result.

				In situ				ATC				Fold test statistics		
	Sector	Sites	Comp	N	D	I	α_{95}	k	D	I	α_{95}	k	f	F	Fold-test result
FT1	N limb	SI17	B	7	173	−56	11	33	313	−65	11	33	BTC: 0.2389	95 per cent = 0.2835	Negative 95 per cent: post-folding
	S limb	SI16		7	183	−70	14	19	305	−88	14	19	ATC: 0.4954		
	N + S	SI16/SI17		14	177	−63	9	21	312	−76	10	17			
FT2	N limb	SI2	B	5	217	−41	21	14	221	−67	21	14	BTC: 0.6772	95 per cent = 0.4542	Negative 99 per cent: post-folding
	S limb	SI4		5	187	−58	10	59	8	−49	10	59	ATC: 3.5873	99 per cent = 0.7783	
	N + S	SI2/SI4		10	205	−51	13	15	339	−76	23	5			
FT3	N limb	SI17	C	8	190	22	17	12	191	−25	17	12	BTC: 0.8189	95 per cent = 0.2386	Positive 95 per cent: pre-folding
	S limb	SI16		8	189	−17	14	16	192	−38	14	16	ATC: 0.088		
	N + S	SI16/SI17		16	190	2	14	8	192	−31	10	14			
FT4	N limb	SI8	C	6	175	20	16	18	16	−81	24	9	BTC: 1.346	95 per cent = 0.43493	Syn-folding. Best statistical solution for 20 per cent unfolding.
	S limb	SI10		6	154	54	12	32	165	14	12	32	ATC: 9.705	99 per cent = 0.5849	
	N + S	SI8/10		12	167	37	14	10	159	−38	44	2	20 per cent unfold. : 0.1334		
FT5	N limb	SI3	C	8	358	21	8	49	345	53	8	49	BTC: 0.8454	95 per cent = 0.2596	Syn-folding. Best statistical solution for 60 per cent unfolding.
	S limb	SI4		7	8	−2	13	22	7	71	13	22	ATC: 0.5761		
	N + S	SI3/4		15	3	10	9	19	352	61	8	22	60 per cent unfold. : 0.1976		

area (Eocene–Oligocene age; Séguret 1972; Teixell 1996; Millán Garrido *et al.* 2000, 2006). Thus, the Eocene–Oligocene reference direction has been calculated for a common reference point located in the centre of the study area (42°41′N, 0°10′W). To calculate the reference direction we used the mean declination and inclination obtained in seven different magnetostratigraphic profiles in the Eocene–Oligocene sediments in the northeastern part of the South-Pyrenean Ebro foreland basin [from sectors 1, 2 and 3 in Taberner *et al.* (1999) and from mean, normal polarity components in the Miralles-La Tossa (Costa *et al.* 2012), Maians-Rubió (Costa *et al.* 2010), Montserrat (Gómez-Paccard *et al.* 2012) and Moia-Santpedor (Costa *et al.* 2011) magnetostratigraphic profiles]. From each of these mean palaeomagnetic directions, and considering the central location of their zones, the palaeopole positions were calculated. Afterwards, the expected declination and inclination was computed from the calculated palaeopoles for the central position of our study area: we obtained a (D/I) of 000°/47° ($N = 7$, $\alpha_{95} = 7°$, $k = 66$).

6 DISCUSSION

6.1 VARs and acquisition time of the B component

The B component shows a constant orientation in geographic coordinates, is reversed in polarity and post-dates folding. This low-temperature component was widely recognized by Oliva-Urcia & Pueyo (2007) throughout the IS and the Bielsa area (Oliva-Urcia *et al.* 2012). The average direction of component B (Dec = 192°, Inc = −45°; $\alpha_{95} = 9°$, $k = 22$, $N = 12$) is different from the Eocene–Oligocene reference direction (Dec = 000°, Inc = 47°) but not the inclination, suggesting a late clockwise VAR in the study area. Combining palaeomagnetic data (considering only sites with $\alpha_{95} \leq 15°$) from the study by Oliva-Urcia & Pueyo (2007) and from this work allows along-strike variation of this rotation to be defined more accurately. The average directions for component B in zones along-strike are in Table 5 and shown in Fig. 15(a). In zone 2, the along-strike data distribution and the stereoplot indicate the presence of two subgroups: in the western zone, the average B component is Dec = 206°, Inc = −37° ($\alpha_{95} = 9.5°$, $k = 24$, $N = 10$); in the eastern zone, the average B component is Dec = 180°, Inc = −50° ($\alpha_{95} = 13°$, $k = 24$, $N = 6$). When compared to the reference (Fig. 15a; Table 5), the average values of this component allow calculation of mean clockwise VARs of +18 (±12°) in zone 1 and +26 (±15.69) in the western part of zone 2. It is important to note that these rotations are small but statistically distinguishable from the Cenozoic reference, and because of its post-folding character, no bias is introduced by tectonic corrections. In the eastern part of zone 2 the average B component is not rotated with respect to the Cenozoic reference whereas in zone 3 the mean B component is slightly rotated anticlockwise (−7 ± 21.7°), although this small rotation is not distinguishable from the reference (Fig. 15a; Table 5). Directions from the western, rotated part of the IS (zones 1 and western part of zone 2) are statistically different from those obtained in the eastern, non-rotated zone (i.e. relative rotations between the two regions are significant, see Fig. 15b).

The mean inclination of component B is similar to the inclination of the Eocene Oligocene reference (47°) in zones 1, 3 and the eastern part of zone 2, but it is slightly shallower in the western part of zone 2. This along-strike variation in the inclination of the B component could indicate that bedding planes had completely acquired their present southwards dip in the western and eastern sectors of the

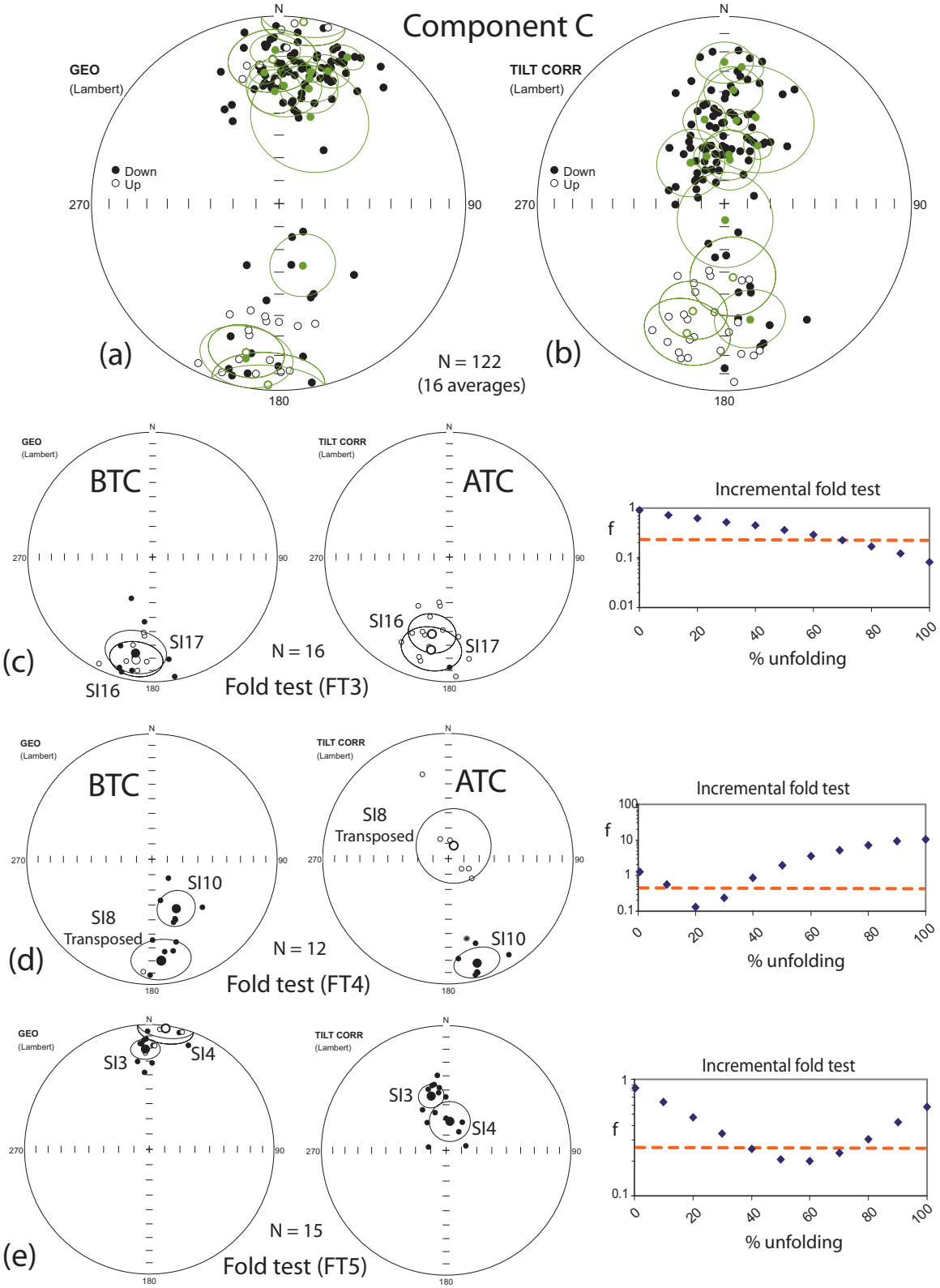

Figure 12. Equal area plots showing the whole dataset of new palaeomagnetic data for component C (a) in geographic coordinates (BTC) and (b) after tectonic correction (ATC). Black, green and orange data are specimen, site mean and total mean palaeomagnetic components. (c–e) Graphical and incremental fold tests (FT3, FT4 and FT5) for component C (see figure caption in Fig. 11). Statistics for the fold test are included in Table 4.

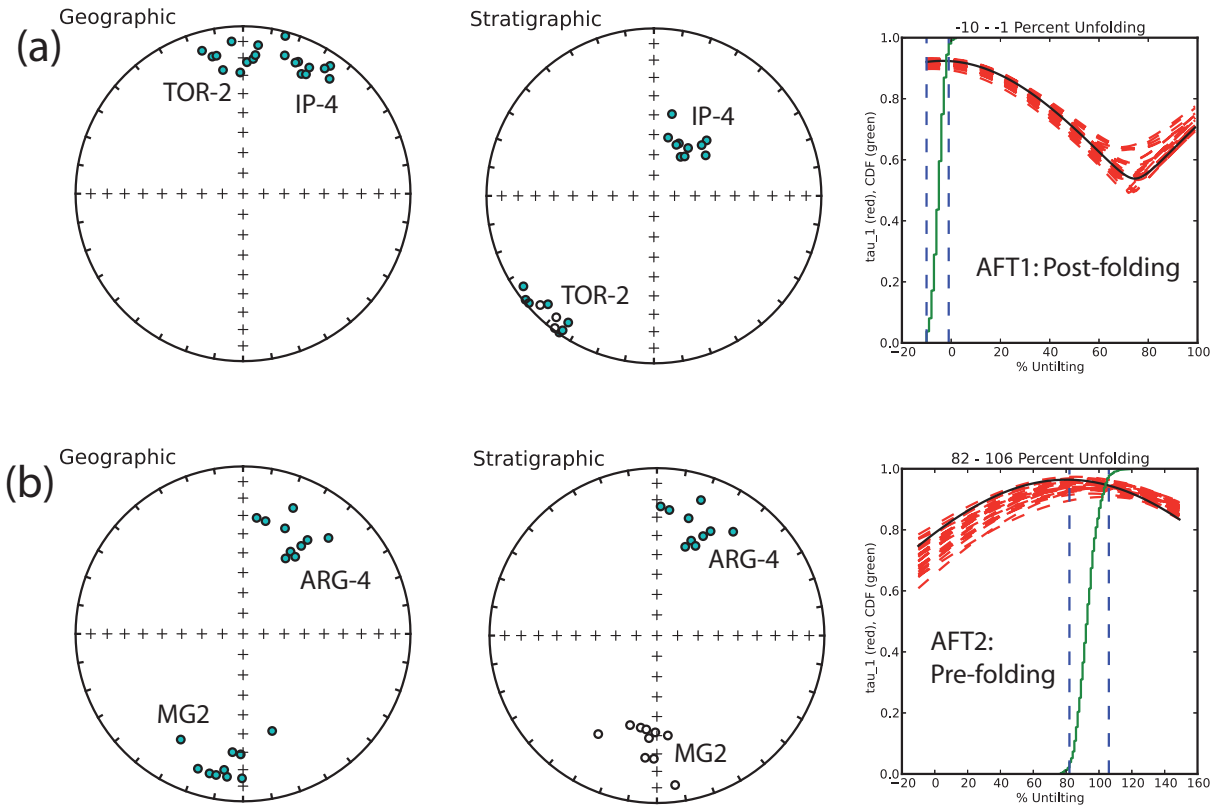

Figure 13. Additional fold tests for the western sector of the IS, using previous palaeomagnetic data by Oliva-Urcia & Pueyo (2007). These previous data are included in Table 3. Fold tests have been carried out using the bootstrap and fold test tools by Tauxe (2010, PmagPy software available from http://earthref.org/PmagPy/cookbook).

study area before acquisition of component B but tilting continued after its acquisition in the central part of the IS. This relationship allows to infer that the acquisition of the B component post-dates emplacement of basement thrust sheets in most of the IS domain although it could be syn-tectonic to the last stages of growth of the AZ anticline in the central part of the IS.

6.2 Acquisition time of the C component

The C component has both normal and reverse polarities and a strong scattering in both geographic and tectonic coordinates (Fig. 11). In spite of showing normal and reverse polarities, it is a secondary component (see conglomerate test results, Fig. 14) and can be interpreted to have different timing relationships with regard to folding along-strike in the study area (see fold test results in Section 5.2).

A more detailed analysis of the structures sampled is needed to understand how C component is related to the structural evolution of the IS. The deformation history of this zone of the Pyrenean range can be summarized as follows (further details on the deformation sequence in the IS and related references can be found in Section 2.2): (i) emplacement of the Larra-Monte-Perdido thin-skinned thrust system, (ii) development of cleavage-related folds affecting the whole stratigraphic sequence (from Palaeozoic up to Cenozoic units) and (iii) passive, kilometric-scale folding of the basement and cover units by basement thrusts. The main basement thrust in the study area is the Gavarnie thrust, which produced the southwards tilting of the stratigraphic sequence in the IS. Towards the eastern part of the study area, the Gavarnie thrust sheet is deformed by the underlying Bielsa (Fig. 1c) and Guara-Gèdre thrusts (Fig. 2c) whereas the Guarga basement thrust (Figs 1b and c) passively transported the entire cover of the South Pyrenean Zone to the south during Oligocene–Miocene times.

The relationships among folding, wholesale deformation linked to basements thrusts and orientation of palaeomagnetic vectors of the C component suggest varied acquisition times for this component with regard to folding and thrusting along the IS (Fig. 16):

(i) For FT3 (see location in Fig. 2a), the C component fits with the Eocene–Oligocene reference for bedding planes unfolded and shallowly dipping to the north (∼10°). This palaeomagnetic component was probably acquired prior to cleavage-related folding but after the early compressional stages (emplacement of the Monte-Perdido thin-skinned thrust system) because bedding was not totally horizontal at the time of acquisition (Fig. 16a). The magnetic field was reversed in polarity when the C component was acquired there.

(ii) For FT4 (see location in Fig. 2a), the C component overlaps the Eocene–Oligocene reference for bedding planes that are folded and rotated Northwards about a horizontal axis with respect to the present-day cross section: bedding in sites SI-8 and SI-10 (to the

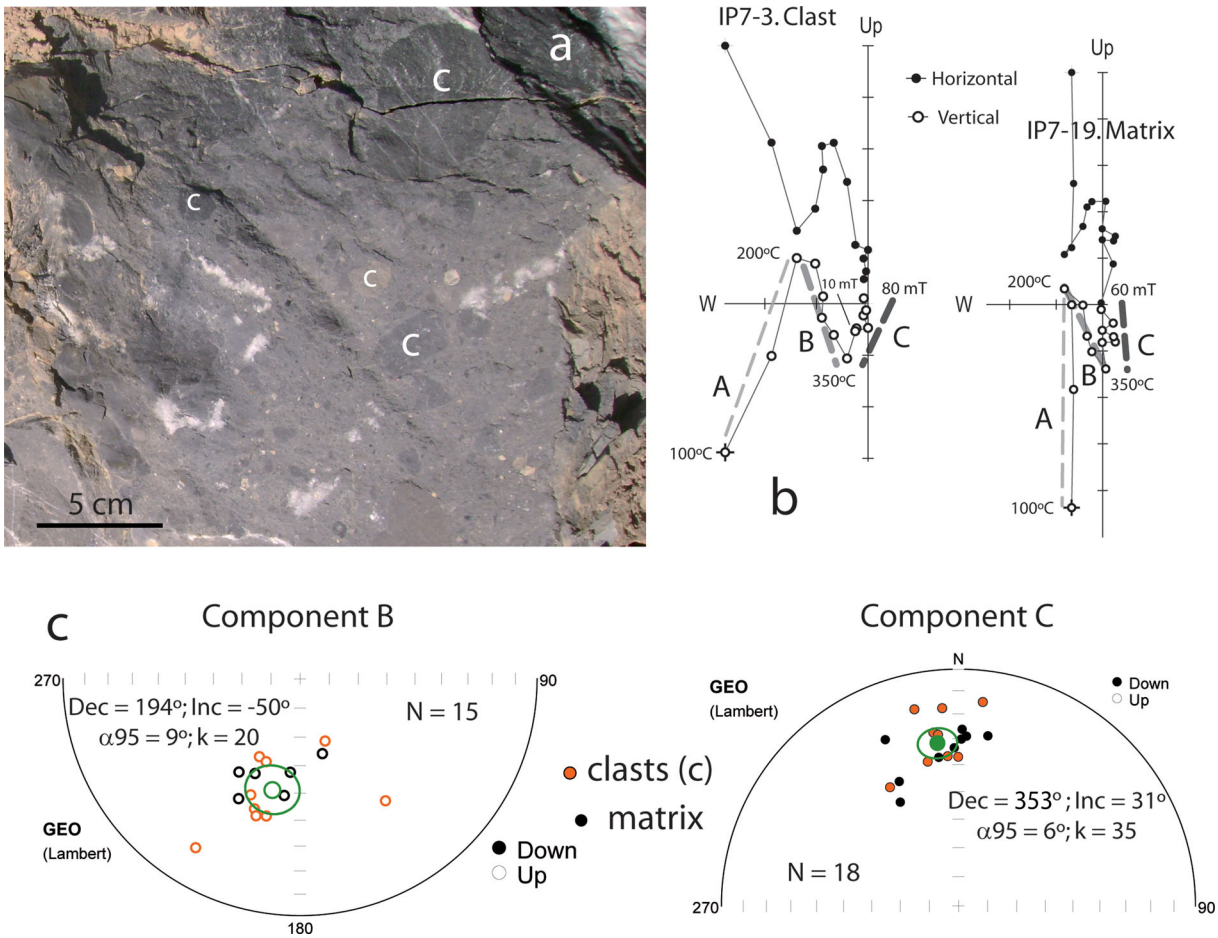

Figure 14. Conglomerate test results in site IP-7. (a) Sampled carbonate mebraccia. (b) Thermal and alternating field demagnetization shown in orthogonal diagrams (geographic coordinates) for representative clast and matrix samples. Segments interpreted as A, B and C components are highlighted. (c) Stereoplots indicating the orientation in geographic coordinates of B and C components, in both clasts and matrix.

Table 5. Rotation of the different structural domains in the IS calculated as the difference in declination between the average palaeomagnetic vector ($D_{obs;}$ observed declination) and the reference vector ($D_{ref;}$ declination of the reference). The errors in the rotation values (ΔR) are calculated as the root sum of the squared errors in the declination of the average palaeomagnetic vector ($\Delta D_{obs} = \alpha_{95}/\cos I_{obs}$) and the reference ($\Delta D_{ref} = 7/\cos 47$).

Zone	D_{obs}	I_{obs}	α_{95}	k	D_{ref}	R	ΔD_{obs} ($\alpha_{95}/\cos I$)	ΔD_{ref}	ΔR
Zone-1	198	−44	4.5	30	000	+18	6.25	10.26	12.01
Zone-2-west	206	−37	9.5	24	000	+26	11.87	10.26	15.69
Zone-2-east	180	−50	13	24	000	0	20.31	10.26	22.75
Zone 3	173	−47	13	16	000	−7	19.12	10.26	21.70

north) should be rotated an average of ∼85º whereas site SI-6 (to the south) requires a rotation of only ∼10º to fit the reference vector. The C component was probably acquired after cleavage-related folding, since bedding was folded before remagnetization, but prior to the emplacement of the basement thrust sheets (Gavarnie and Guara-Gèdre in this area), which gave rise to the passive folding of cover units and southwards rotation of bedding (Fig. 16b). The time span for the acquisition of the C component in this structure includes chrons of both, normal and reverse polarity magnetic fields.

(iii) For FT5 (see location in Fig. 2a), the C component fits with the Eocene–Oligocene reference for bedding planes that are slightly folded and dip shallowly to the south (∼10ºS in site SI-3 and ∼25ºS in site SI-4). The present-day dip is higher, 36ºS for SI-3 and 73ºS for SI-4, and thus, indicates that there was an additional Southwards tilt of bedding planes of ∼25º and ∼50º, respectively, after the acquisition of the C component, related to the growth of the kilometric-scale anticline in the hangingwall of the Gavarnie basement thrust (Fig. 16c). The C component was probably acquired before emplacement of the Gavarnie basement thrust sheet, during a period of normal polarity magnetic field for sites SI-3 and SI-4 (nonetheless, a reverse polarity component was obtained in site SI-1, located about 1 km to the west of SI-3).

(iv) For AFT1 (see location in Fig. 2a), the C component overlaps the Eocene–Oligocene reference when bedding planes are folded but rotated northwards with respect to their present-day attitude: bedding in sites TOR-2 and IP-4 should be rotated ∼25–30º respectively to fit the Eocene–Oligocene reference vector. These rotations equal the passive folding of cover units due to the emplacement of the Gavarnie basement thrust sheet, which produced an average

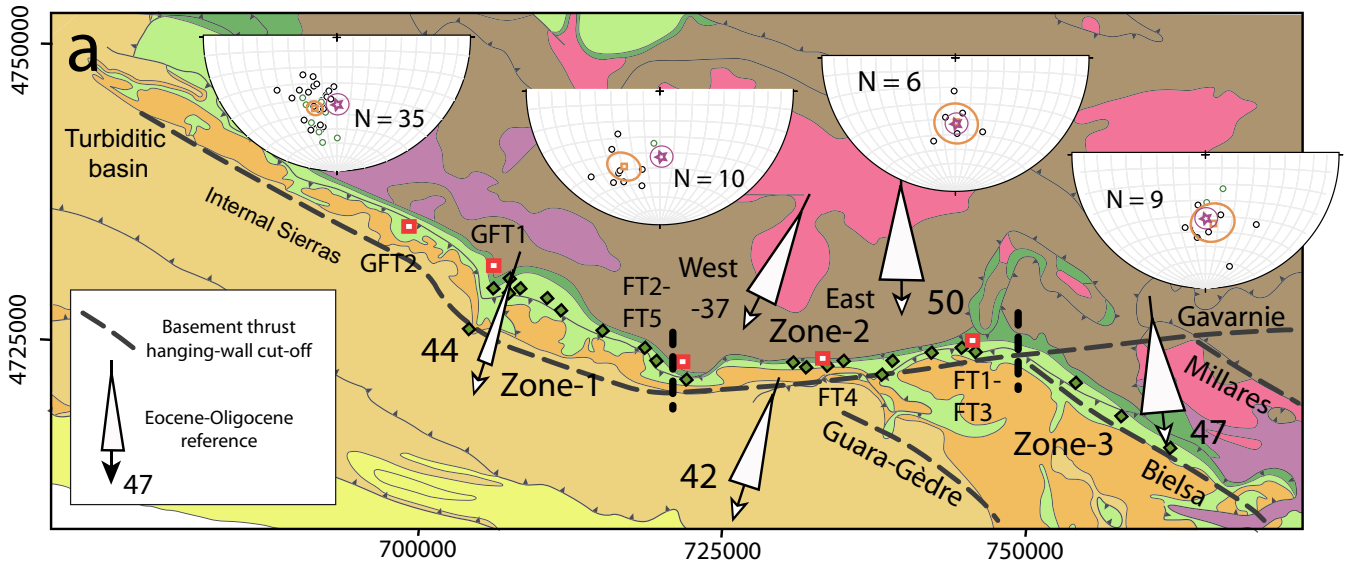

b

	Zone-2-West	Zone-2-East	Zone-3
Zone-1	c.a. (9.82) > o.a. (9.62) Non-statist. disting.	c.a. (11.99) < o.a. (13.62) Statist. disting.	c.a. (10.84) < o.a. (17.7) Statist. disting.
Zone-2-West		c.a. (16.04) < o.a. (22.72) Statist. disting.	c.a. (15.76) < o.a. (26.24) Statist. disting.
Zone-2-East			c.a. (18.81) > o.a. (5.52) Non-statist. disting.

Figure 15. (a) Along-strike distribution of the B component in the IS (green dots are site means from this study, black dots from Oliva-Urcia & Pueyo 2007). In the stereoplots, the violet star marks the expected reverse polarity direction. Red dots indicate the average palaeomagnetic vector for each considered zone. White arrows represent the declination (and corresponding α_{95}) of the mean palaeomagnetic vectors defined for each structural domain (the white arrow in the legend refers to the Eocene-Oligocene reference direction). Accompanying numbers indicate inclinations. (b) Comparison of each zone average direction to the average directions obtained in the other three domains. McFadden & McElhinny (1990) statistics were applied to define if directions are (green colour) or are not (red colour) statistically distinguishable. From the application of the test (Super IAPD2000 software, Torsvik *et al.* 2000) two angles are derived: the critical angle (c.a. in the table) at which the hypothesis of common mean direction can be rejected at the 95 per cent confidence level, and the observed angle (o.a.). If the observed angle is higher than the critical angle the two directions cannot share a common mean direction and are therefore statistically distinguishable.

southwards tilt of 20–25° in this sector of the IS (Teixell *et al.* 1989, see Fig. 16d). Therefore, the C component was acquired prior to the emplacement of the Gavarnie basement thrust but after cleavage-related folding since beds were already folded when the remagnetization occurred. The magnetic field was normal in polarity when the C component was acquired.

(v) For AFT2 (see location in Fig. 2a), the C component fits with the Eocene–Oligocene reference when bedding planes are unfolded and horizontal (MG2 in the northern limb) or slightly dipping to the north (25°N in ARG-4 in the southern limb). The C component was acquired prior to cleavage-related folding but after the early compressional stages (development of the Larra thrust system) because bedding was already slightly deformed in site ARG-4 (Fig. 16e). MG2, in the northern limb, is located below the main detachment level of the Larra thrust system and, accordingly to our interpretation, beds were not tilted in this site when the remagnetization occurred. The time span for the acquisition of the C component includes chrons of both normal and reverse polarity magnetic field.

The C component was also recognized by Oliva-Urcia & Pueyo (2007) but their interpretation differed from the interpretation given in the present work: they considered that this palaeomagnetic component had a primary origin based on (i) the observation of normal and reverse polarities along the IS and (ii) the results at regional scale of the McElhinny (1964) fold test, that indicated a pre-folding acquisition for this component. One of the aims of the present work was to carry out a more detailed analysis of this component, and in order to achieve this objective we performed a conglomerate test and analysed the acquisition time for the C component not at the regional scale but in particular structures, where the geometrical relationship between thrusting and cleavage-related folding is well defined from previous geological cross sections and structural studies (Ríos Aragüés *et al.* 1972; Labaume *et al.* 1985; Ríos-Aragüés *et al.* 1987a,b; Teixell & García Sansegundo 1989; Teixell *et al.* 1989; Alonso & Teixell 1992; Teixell 1992; Rodríguez-Méndez *et al.* 2013; Izquierdo-Llavall *et al.* 2013a). Furthermore, the combined use of thermal and AF demagnetization was successful and permitted detection of the C component in a higher percentage of

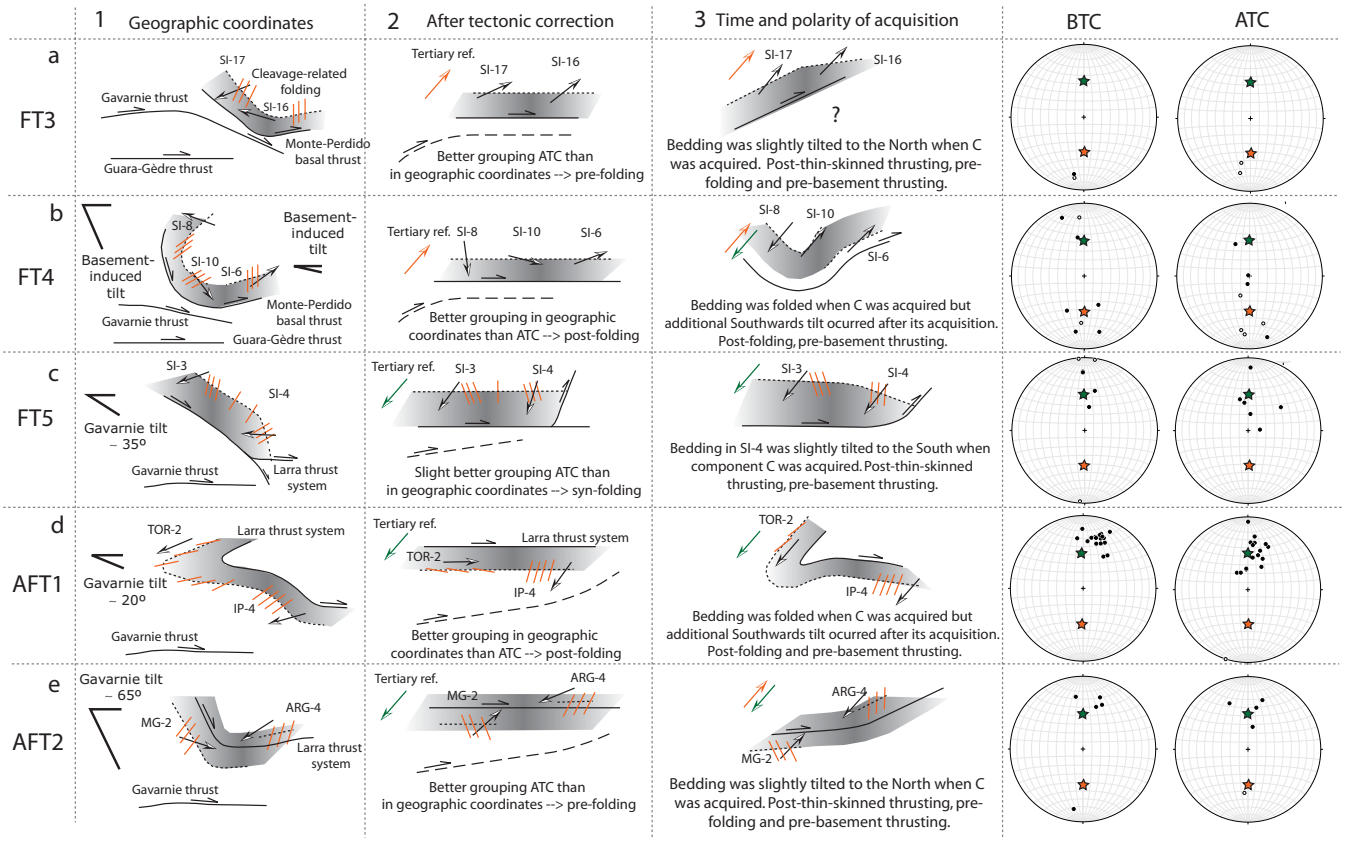

Figure 16. Geological sketch of the folds analysed in Section 5.2 with indication of the orientation of bedding (black) and cleavage (orange) in each site considered, the orientation of the C component and the attitude of the main cover (Larra-Monte-Perdido) and basement thrusts (Gavarnie and Guara-Gèdre thrusts). For each structural situation, (1) the schematic present-day N–S cross section and orientation of the C component in geographic coordinates, (2) a simple restoration of the cross section with the orientation of the C component after tectonic correction and, finally, (3) the expected orientation of bedding and cleavage for the time the C component was acquired (i.e. bedding, cleavage and the C component are rotated around an E–W-trending, horizontal axis to fit the palaeomagnetic component with the reference direction) are shown. Plots to the right show the orientation of C component for all sites located in the area of the structure considered (data from this study and from Oliva-Urcia & Pueyo 2007). Orange/green was used for reverse/normal polarity.

samples than in the previous study by Oliva-Urcia & Pueyo (2007) where only thermal demagnetization was used. These new considerations allowed us to determine that the C component is not primary but rather is a remagnetized component showing a complex, syn-deformation character. Taking into account data from Oliva-Urcia & Pueyo (2007) and from this study (and grouping them in sectors coinciding with the fold tests in Section 5.2), the stereoplots in Fig. 16 were constructed (FT3, FT4, FT5, AFT1 and AFT2): in FT4 and FT5, the components are not well grouped neither in geographic nor in stratigraphic coordinates; in AFT1 the C components show a better grouping in geographic coordinates, with a small dispersion in the declination, but the inclination of the mean vector is shallower than the Eocene–Oligocene reference; in AFT2, the components are better grouped after tectonic correction but show a small dispersion in inclination, that is consistent with the existence of an early deformation of bedding before the C component was acquired. Most data (from all sites in this study and the study by Oliva-Urcia & Pueyo 2007) correspond to the AFT1 area, where the mean C component is (in geographic coordinates) Dec = 017°, Inc = 30° ($\alpha_{95} = 5°$, $k = 44$, $N = 17$). In order to calculate VARs using these data, it is necessary to restore them to the time of acquisition (i.e. in this particular area, before the ∼20° southwards tilting induced by the Gavarnie thrust sheet). This means that data should be tilted 20° northwards using the average fold axis for the Gavarnie hangingwall anticline in this area (∼110, 00). After this rotation the average C component in the AFT1 area is Dec = 015°, Inc = 50° ($\alpha_{95} = 5°$, $k = 44$, $N = 17$). This component fits the inclination of the Eocene–Oligocene reference and is clockwise rotated an average of +15° (±12.87°) which is consistent with the average rotation of +18 (±12°) calculated for the B component in this zone (zone 1, see Fig. 15a). The good agreement between both rotations (in spite of the high error values) supports clockwise VAR after acquisition of the B component with no significant rotation in the interval between C and B remagnetizations: the rotation is late in the deformation history of the IS, possibly during the late deformation of the Gavarnie thrust due to the emplacement of the Guarga thrust sheet (Oliva-Urcia & Pueyo 2007) (see cross-sections in Figs 1b and c) and the Guara-Gèdre and Bielsa thrusts.

6.3 Evolutionary model and tectonic implications

The Larra-Monte Perdido thrust system was active during Mid-Late Lutetian to Bartonian times according to tectonics-sedimentation relationships (Remacha *et al.* 1987; Barnolas *et al.* 1991; Teixell 1992). The Gavarnie basement thrust developed during Early-Middle Priabonian to Rupelian times in the western part of the study area (Teixell 1992) and during Early Bartonian to Mid Rupelian towards the eastern part (Millán-Garrido *et al.* 2006). It is deformed by the Bielsa (Fig. 1b), Guara-Gèdre (Fig. 2c) and Guarga (Figs 1b

and c) thrusts. The latter was active during the Late Oligocene and Miocene (Pocoví *et al.* 1990; Teixell 1996; Millán-Garrido *et al.* 2000). Cleavage related folding in the IS post-dates emplacement of the Larra-Monte-Perdido thin-skinned thrust system and palaeomagnetic data support that it predates (or is early with regard) the southwards tilt of the IS produced by the growth of the Gavarnie hangingwall anticline.

The two remagnetization events interpreted in this study occurred during different stages of the Cenozoic Pyrenean compression and totally erased the primary signal in the analysed rocks. Because of the particular conditions of the Pyrenean basins, a chemical mechanism for remagnetization, linked to remobilization of iron during the orogenic period and in relation to sedimentary and/or tectonic load and migration of orogenic fluids can be considered (Oliver 1986; McCabe & Elmore 1989; Jackson 1990; Banerjee *et al.* 1997; Oliva-Urcia & Pueyo 2007; Oliva-Urcia *et al.* 2008; Aubourg *et al.* 2012; Muñoz *et al.* 2013). The history of the study area can be portrayed as "lines" of relative chronology shown in Fig. 17, assuming the previously mentioned time brackets for the different deformation events and taking into account (i) the relative chronology between remagnetization and structures inferred from the restoration of palaeomagnetic data (see Sections 5.2, 6.1 and 6.2) and (ii) the observed magnetic field polarities.

The older remagnetization event (C component) was diachronous through the study area, since normal and reverse polarities are recognized, and was acquired in different deformation stages depending on the structural position of the sites (Figs 16 and 17): it is pre-cleavage related folding but probably syn- or post-thin skinned thrusting in FT3 (reverse polarity) and AFT2 (normal and reverse polarities) but post-folding (or late syn-folding) and pre-Gavarnie thrust in FT4 (reverse and normal polarities), FT5 (normal and reverse polarities) and AFT1 (normal polarity). In general terms, the C component has a dominant reverse polarity towards the eastern part of the IS and a dominant normal polarity towards its western part. Considering the geomagnetic polarity time scale (GPTS) for the Lutetian-Priabonian, and the age of deformation, this along-strike variation in the polarity of the C component suggests that it could have been acquired mainly during the C19 chron or the lower part of C18 chron (reverse polarities are dominant) to the east and during the upper part of the C18 chron or during C17 or C16 chrons (normal polarities are dominant) to the west. Remagnetization was probably simultaneous with the maximum burial and peak temperature conditions in the IS (160–190 °C, Izquierdo-Llavall *et al.* 2013a), which favoured iron mobilisation. The C remagnetized component defined in this work is consistent with the remagnetization found by Muñoz *et al.* (2013) in the Ainsa oblique zone, in the western margin of the SPCU (see location in Fig. 1a). In this area, normal and reverse polarity remagnetizations were observed and showed moderate values of clockwise rotation that are lower than those defined from the primary magnetization in closely located sites. Considering the age of rotation in the western part of the SPCU, these authors proposed that remagnetization took place during Middle-Late Eocene times, accordingly with the age inferred for the C component in the IS.

The younger remagnetization event (B component) has been interpreted to post-date basement-induced tilting in the IS except in the western part of zone 2 (see location in Fig. 2a), where it may be coeval with the last stages of growth of the AZ anticline. Component B was assigned by Oliva-Urcia & Pueyo (2007) to the C12R chron, which is the longest reverse polarity chron in the Rupelian. In general terms, this component does not show VARs (or is slightly rotated anticlockwise) in the east, but does show small, statistically significant clockwise rotations to the west (+18° in zone 1 and +26° in the western part of zone 2). The comparison of these late rotations to the rotations inferred from the C component indicates that, at least for zone 1, no significant VAR occurred between the last stages of folding and the acquisition of the B component. Rotations in the western sector of the IS are the result of the westwards decrease in the shortening associated with the basement thrust system below the Gavarnie unit (Bielsa, Guara-Gèdre and Guarga thrusts, see Figs 1b and c and Figs 15a and 17). The Guarga basement thrust is continuous along the study area, but the Bielsa and Guara-Gèdre thrusts are smaller-scale thrust sheets that are limited to the eastern margin of the IS and end laterally to the west (Fig. 17). The additional shortening to the east associated with these thrusts (and perhaps the westwards shortening decrease in the Guarga basement thrust) control the occurrence of clockwise VARs in the western part of the IS.

Taking into account these rotations, we can tentatively reconstruct (Fig. 17) the orientation of the southern front of the IS after restoring the VARs calculated from component B. The resulting geometry (see Fig. 17) indicates that the IS do not result from VARs of an initially linear structure. On the contrary, their originally curved front could be related to an inherited basement geometry (assuming no rotation occurred prior to the acquisition of the remagnetized palaeomagnetic components) that was reactivated by basement thrusts during the Pyrenean compression: its western and eastern fragments (zones 1 and 3) could be NW–SE to WNW–ESE-striking structures that were connected by a slightly oblique structure, striking NE–SW in its central part (zone 2). These fault strikes (N110°E and N060°E) were recognized by Bixel & Lucas (1983) in the pre-orogenic sequence to the south of the Western Axial Zone, related to basin configuration and magmatism during Stephanian-Permian times (Bixel & Lucas 1983).

7 CONCLUSIONS

The new palaeomagnetic data presented in this work allow for the first time two remagnetization events to be distinguished in the Upper Cretaceous units (Marboré and Zuriza Fms.) of the Pyrenean IS. These events are represented by two stable components: a lower-temperature, reverse component (B) that post-dates folds and basement thrusting, and a higher-temperature component (C) that was successfully isolated by a combined thermal and AF demagnetization technique. The results from a conglomerate test on clasts and matrix in the lower Eocene syn-tectonic deposits of the Jaca basin, as well as the careful analysis of the C component in particular structures, support the reinterpretation of this component as an early remagnetization that is pre- to post-folding in different areas, but everywhere pre-dates tilting induced by the emplacement of basement thrust sheets below the IS (the Gavarnie thrust mainly). This remagnetization is diachronous along the IS: it is dominantly reversed in polarity to the east but dominantly normal to the west.

The B component shows small but statistically significant clockwise rotations in the western part of the IS (from +18 to +26°) that are similar to the rotations calculated (when possible) from the C component. These rotations can be attributed to the westwards shortening decrease in the thrust system below the Gavarnie unit that is result of its along-strike structural change, with a higher number of basement thrusts to the east. According to the results obtained, the along-strike change in the trend of the IS could be interpreted as the result of basement geometrical features inherited from previous times (Variscan Orogeny, Late Variscan tectonics or Mesozoic extension).

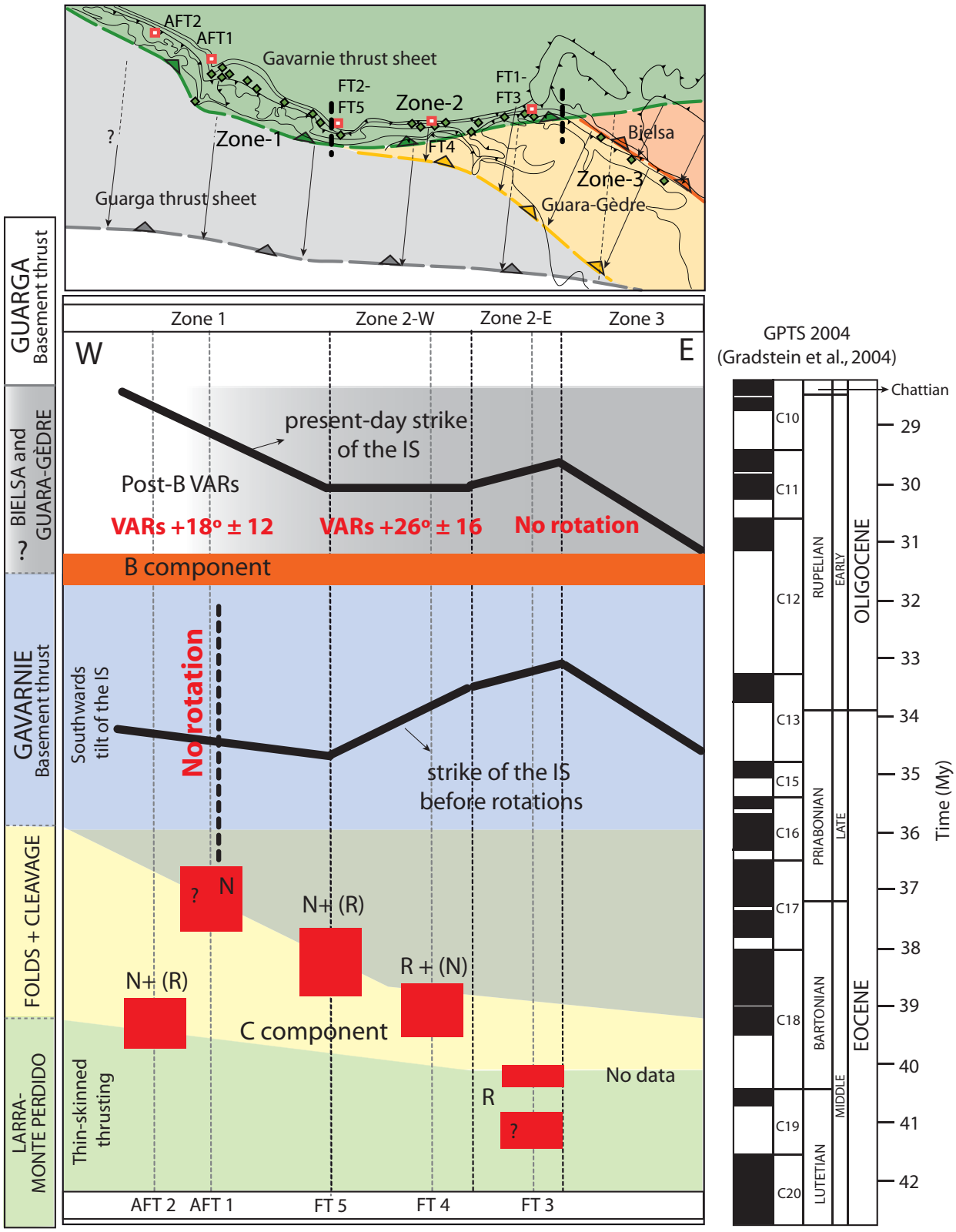

Figure 17. Summary of palaeomagnetic and rotational results along the strike of the IS with interpretation of the relative chronology between remagnetization events (components B and C) and deformation stages. The age of deformation and related geomagnetic polarity time scale (Gradstein *et al.* 2004) are shown. The map in the upper part of the figure includes the location of the hanging-wall cut offs of basement thrusts (Gavarnie, Guarga, Bielsa and Guara-Gèdre).

ACKNOWLEDGEMENTS

The authors thank Elisa Sánchez, Cristina García, Pablo Calvín, Pablo Santolaria, Roi Silva y Miguel Gallego for their help during field work. This work is part of the research projects CGL2009-08969 and CGL2006-05817 (Spanish Ministry of Education) and is included in the objectives of the pre-doctoral grant AP-2009 – 0554 (Esther Izquierdo, Programa de formación de profesorado universitario, Spanish Ministry of Education). BOU acknowledges founding from the JAEDOC program of CSIC and ESF. Careful revisions from Rob Van der Voo and Chris Rowan are also acknowledged.

REFERENCES

Allerton, S., 1998. Geometry and kinematics of vertical-axis rotations in fold and thrust belts, *Tectonophysics,* **299,** 15–30.

Allmendinger, R.W., Cardozo, N.C. & Fisher, D., 2013. *Structural Geology Algorithms: Vectors & Tensors,* Cambridge Univ. Press, 289 pp.

Alonso, JL. & Teixell, A., 1992. Forelimb deformation in some natural examples of fault-propagation folds, in *Thrust Tectonics,* pp. 175–180, ed. McClay, K.R., Chapman & Hall.

Aubourg, C., Pozzi, J.P. & Kars, M., 2012. Burial, claystones remagnetization and some consequences for magnetostratigraphy, *Geol. Soc., Lond., Spec. Publ.,* **371,** 181–188.

Banerjee, S., Elmore, R.D. & Engel, M.H., 1997. Chemical remagnetization and burial diagenesis: testing the hypothesis in the Pennsylvanian Belden Formation, Colorado, *J. geophys. Res.,* **102**(B11), 24 825–24 842.

Barnolas, A. & Teixell, A., 1994. Platform sedimentation and collapse in a carbonate-dominated margin of a foreland basin (Jaca basin, Eocene, southern Pyrenees), *Geology,* **22**(12), 1107–1110.

Barnolas, A., Samsó, J.M., Teixell, A., Tosquella, J. & Zamorano, M., 1991. Evolución sedimentaria entre la cuenca de Graus-Tremp y la cuenca de Jaca-Pamplona. Congreso Grupo Español del Terciario, Libro-Guía Excursión nº 1, Vic, 123 pp.

Bates, M., 1989. Palaeomagnetic evidence for rotations and deformation in the Nogueras Zone. Central Southern Pyrenees, *J. Geol. Soc. Lond.,* **146,** 459–476.

Bixel, F. & Lucas, C.L., 1983. Magmatisme, tectonique et sédimentation dans les fossés stéphano-permiens des Pyrénées occidentales, *Revue de Géologie Dynamique et Géographie Physique,* **24,** 329–342.

Cardozo, N. & Allmendinger, R.W., 2013. Spherical projections with OSX Stereonet, *Comput. Geosci.,* **51,** 193–205.

Chadima, M. & Hrouda, F., 2006. Remasoft 3.0 a user-friendly paleomagnetic data browser and analyzer, *Travaux Géophysiques,* **27,** 20–21.

Channell, J.E.T. & McCabe, C., 1994. Comparison of magnetic hysteresis parameters of unremagnetized and remagnetized limestones, *J. geophys. Res.,* **99,** 4613–4623.

Cogné, J.P., 1987. Paleomagnetic direction obtained by strain removal of Pyrenean Permian redbeds at the "Col du Somport" (France), *Earth planet. Sci. Lett.,* **85,** 162–172.

Costa, E., Garcés, M., López-Blanco, M., Beamud, E., Gómez-Paccard, M. & Larrasoaña, J.C., 2010. Closing and continentalization of the South Pyrenean foreland basin (NE Spain): magnetochronological constraints, *Basin Res.,* **22,** 904–917.

Costa, E., Garcés, M., Sáez, A., Cabrera, L. & López-Blanco, M., 2011. The age of the "Grande Coupure" mammal turnover: new constraints from the Eocene–Oligocene record of the Eastern Ebro Basin (NE Spain), *Palaeogeogr., Palaeoclimatol., Palaeoecol.,* **301,** 97–107.

Costa, E., Garcés, M., López-Blanco, M., Serra-Kiel, J., Bernaola, G., Cabrera, L. & Beamud, E., 2012. The Bartonian-Priabonian marine record of the eastern South Pyrenean Foreland Basin (NE Spain): a new calibration of the larger foraminifers and calcareous nannofossil biozonation, *Geol. Acta,* **11**, 177–193.

Day, R., Fuller, M. & Schmidt, V.A., 1977. Hysteresis properties of titanomagnetites: grain-size and compositional dependence, *Phys. Earth planet. Inter.,* **13,** 260–267.

Dinarès, J., McClelland, E. & Santanach, P., 1992. Contrasting rotations within thrust sheets and kinematics of thrust tectonics as derived from palaeomagnetic data: an example from the Southern Pyrenees, in *Thrust Tectonics,* pp. 235–246, ed. McClay, K.R., Chapman & Hall.

Dunlop, D.J., 1972. Magnetic mineralogy of unheated and heated red sediments by coercivity spectrum analysis, *Geophys. J. R. astr. Soc.,* **27,** 37–55.

Dunlop, D.J., 2002. Theory and application of the Day plot (Mrs/Ms versus Hcr/Hc) 2. Application to data for rocks, sediments and soils, *J. geophys. Res.,* **107** (B3), EPM 5-1–EPM 5-15.

Enkin, R.J., Osadetz, K.G., Baker, J. & Kisilevsky, D., 2000. Orogenic remagnetizations in the Front Ranges and Inner Foothills of the southern Canadian Cordillera: chemical harbinger and thermal handmaiden of Cordilleran deformation, *Geol. Soc. Am. Bull.,* **112,** 929–942.

Fisher, R.A., 1953. Dispersion on a sphere, *Proc. R. Soc. Lond.,* **217,** 295–305.

Fournier, E., 1905. Études géologiques sur la partie occidentale de la chaîne des Pyrénées entre la vallée d'Aspe et le celle de la Nive, *Bull. Soc. Geol. Fr.,* **5,** 699–723.

Gómez-Paccard, M., López-Blanco, M., Costa, E., Garcés, M., Beamud, E. & Larrasoaña, J.C., 2012. Tectonic and climatic controls on the sequential arrangement of an alluvial fan/fan-delta complex (Montserrat, Eocene, Ebro Basin, NE Spain), *Basin Res.,* **24,** 437–455.

Gradstein, F.M., Ogg, J.G. & Smith, A.G., 2004. *Geologic Time Scale 2004,* Cambridge Univ. Press, 589 pp.

Henry, B., Rouvier, H. & LeGoff, M., 2004. Using syntectonic remagnetizations for fold geometry and vertical axis rotation: the example of the Cévennes border (France), *Geophys. J. Int.,* **157,** 1061–1070.

Holl, J.E. & Anastasio, D.J., 1995. Cleavage development within a foreland fold and thrust belt, southern Pyrenees, Spain, *J. Struct. Geol.,* **17**, 357–369.

Housen, B.A. *et al.*, 2003. Paleomagnetism of the Mount Stuart Batholith revisited again: what has been learned since 1972?, *Am. J. Sci.,* **303,** 263–299.

Izquierdo-Llavall, E., Aldega, L., Cantarelli, V., Corrado, S., Gil-Peña, I., Invernizzi, C. & Casas, A.M., 2013a. On the origin of cleavage in the Central Pyrenees: structural and paleo-thermal study, *Tectonophysics,* **608,** 303–318.

Izquierdo-Llavall, E., Casas-Sainz, A. & Gil-Peña, I., 2013b. Estructura de las Sierras Interiores en la Zona Surpirenaica (valles del Aragón y del Osia, Pirineos Centrales): implicaciones en la cronología de la deformación, *Geogaceta,* **53,** 57–60.

Izquierdo-Llavall, E., Casas-Sainz, A., Oliva-Urcia, B. & Scholger, R., 2014. Palaeomagnetism and magnetic fabrics of the Late Palaeozoic volcanism in the Castejón-Laspaúles basin (Central Pyrenees). Implications for palaeoflow directions and basin configuration, *Geol. Mag.,* **151**(05), 777–797.

Jackson, M., 1990. Diagenetic sources of stable remanence in remagnetized Paleozoic cratonic carbonates: a rock magnetic study, *J. geophys. Res.,* **95,** 2753–2761.

Jordanova, N., Henry, B., Jordanova, D., Ivanov, Z., Dimov, D. & Bergerat, F., 2001. Paleomagnetism in northwestern Bulgaria: geological implications of widespread remagnetization, *Tectonophysics,* **343,** 79–92.

Kirschvink, J.L., 1980. The least-squares line and plane and the analysis of paleomagnetic data, *Geophys. J. R. astr. Soc.,* **62,** 699–718.

Kruiver, P.P., Dekkers, M.J. & Heslop, D., 2001. Quantification of magnetic coercivity by analysis of acquisitions curves of isothermal remanent magnetisation, *Earth planet. Sci. Lett.,* **189,** 269–76.

Labaume, P., Mutti, E., Séguret, M. & Rossell, J., 1983. Mégaturbidites carbonatées du bassin turbiditique de l'Eocène inférieur et moyen sud-pyrénéen, *Bull. Soc. Geol. Fr.,* **6,** 927–941.

Labaume, P., Séguret, M. & Seyve, C., 1985. Evolution of a turbiditic foreland basin and analogy with an accretionary prism: example of the Eocene south Pyrenean basin, *Tectonics,* **4,** 661–685.

Lewchuk, M.T., Douglas Elmore, R. & Evans, M., 2002. Remagnetization signature of Paleozoic sedimentary rocks from the Patterson Creek Mountain anticline in West Virginia, *Phys. Chem. Earth,* **27,** 1141–1150.

Lowrie, W., 1990. Identification of ferromagnetic minerals in a rock by coercivity and unblocking temperature properties, *Geophys. Res. Lett.,* **17,** 159–162.

Martínez-Peña, M.B. & Casas-Sainz, A.M., 2003. Cretaceous-Tertiary tectonic inversion of the Cotiella Basin (southern Pyrenees, Spain), *Int. J. Earth Sci.,* **92,** 99–113.

McCabe, C. & Elmore, R.D., 1989. The occurrence and origin of late Paleozoic remagnetization in the sedimentary rocks of North America, *Rev. Geophys.,* **27,** 471–494.

McClelland, E.A. & McCaig, A.M., 1989. Palaeomagnetic estimates of rotation in basement thrust sheets, Axial Zone, Southem Pyrenees, *Cuadernos de Geología Ibérica,* **12,** 181–193.

McElhinny, M.W., 1964. Statistical significance of the fold test in paleomagnetism, *Geophys. J. R. astr. Soc.,* **8,** 338–340.

McFadden, P.L. & Jones, D.L., 1981. The fold test in palaeomagnetism, *Geophys. J. R. astr. Soc.,* **67,** 53–58.

McFadden, P.L. & McElhinny, M.W., 1990. Classification of the reversal test in palaeomagnetism, *Geophys. J. Int.,* **103**, 725–729.

Millán, H., Pueyo, E.L., Aurell, M., Luzón, A., Oliva, B., Martínez-Peña, M.B. & Pocoví, A., 2000. Actividad tectónica registrada en los depósitos terciarios del frente meridional del Pirineo central, *Rev. Soc. Geol. Esp.,* **13,** 279–300.

Millán-Garrido, H., Oliva Urcia, B. & Pocoví Juan, A., 2006. La transversal de Gavarnie-Guara. Estructura y edad de los mantos de Gavarnie, Guara-Gèdre y Guarga (Pirineo centro-occidental), *Geogaceta,* **40,** 35–38.

Mochales, T., Casas, A.M., Pueyo, E.L. & Barnolas, A., 2012. Rotational velocity for oblique structures (Boltaña anticline, Southern Pyrenees), *J. Struct. Geol.,* **35,** 2–16.

Muñoz, J.A., 1992. Evolution of a continental collision belt: ECORS Pyrenees crustal balanced section, in *Thrust Tectonics,* pp. 235–246, ed. McClay, K.R., Chapman & Hall.

Muñoz, J.A., Beamud, E., Fernández, O., Arbués, P., Dinarès-Turell, J. & Poblet, J., 2013. The Ainsa Fold and thrust oblique zone of the central Pyrenees: kinematics of a curved contractional system from paleomagnetic and structural data, *Tectonics,* **32,** 1142–1175.

Mutti, E., 1977. Distinctive thin-bedded turbidite facies and related environments in the Eocene Hecho Group (south-central Pyrenees, Spain), *Sedimentology,* **24,** 107–131.

Mutti, E., Luterbacher, H., Ferrer, J. & Rosell, J., 1972. Schema stratigrafico e lineamenti di facies del Paleogeno Marino della zona centrale sudpirenaica tra Tremp (Catalogna) e Pamplona (Navarra), *Mem. Soc. Geol. Ital.,* **18,** 15–22.

Muttoni, G., 1995. "Wasp-waisted" hysteresis loops from a pyrrhotite and magnetite-bearing remagnetized Triassic limestone, *Geophys. Res. Lett.,* **22,** 3167–3170.

Oliva-Urcia, B., 2004. Geometría y cinemática rotacional en las Sierras Interiores y Zona Axial (sector de Bielsa) a partir del análisis estructural y paleomagnético, *PhD thesis,* Unpublished, University of Zaragoza 290 pp.

Oliva-Urcia, B. & Pueyo, E.L., 2007. Rotational basement kinematics deduced from remagnetized cover rocks (Internal Sierras, southwestern Pyrenees), *Tectonics,* **26,** TC4014, doi:10.1029/2006TC001955.

Oliva-Urcia, B., Pueyo, E.L. & Larrasoaña, J.C., 2008. Magnetic reorientation induced by pressure solution: a potential mechanism for orogenic-scale remagnetizations, *Earth planet. Sci. Lett.,* **265,** 525–534.

Oliva-Urcia, B., Casas, A.M., Pueyo, E.L., Román-Berdiel, T. & Geissman, J.W., 2010. Paleomagnetic evidence for dextral strike-slip motion in the Pyrenees during alpine convergence (Mauléon basin, France), *Tectonophysics,* **494,** 165–179.

Oliva-Urcia, B., Pueyo, E.L., Larrasoaña, J.C., Casas, A.M., Román-Berdiel, T., Van der Voo, R. & Scholger, R., 2012. New and revisited paleomagnetic data from Permian-Triassic red beds: two kinematic domains in the west-central Pyrenees, *Tectonophysics,* **522–523,** 158–175.

Oliver, J., 1986. Fluids expelled tectonically from orogenic belts: their role in hydrocarbon migration and other geologic phenomena, *Geology,* **14,** 99–102

Pocoví, A., Millán, H., Navarro, J.J. & Martínez Peña, M.B., 1990. Rasgos estructurales de la Sierra de Salinas y zona de los Mallos (Sierras Exteriores, Prepirineo, provincias de Huesca y Zaragoza, *Geogaceta,* **8,** 36–39.

Pueyo, E.L., Millán, H. & Pocoví, A., 2002. Rotation velocity of a thrust: a paleomagnetic study in the External Sierras (Southern Pyrenees), *Sediment. Geol.,* **146,** 191–208.

Pueyo, E.L., Pocoví, A., Millán, H. & Sussman, A.J., 2004. Map-view models for correcting and calculating shortening estimates in rotated thrust fronts using paleomagnetic data, in *Orogenic Curvature: Integrating Paleomagnetic and Structural Analyses,* Vol. 383, pp. 55–71, eds Sussman, A.J. & Weil, A.B., Spec. Pap. Geol. Soc. Am.

Pueyo, E.L., Mauritsch, H.J., Gawlick, H.J., Scholger, R. & Frisch, W., 2007. New evidence for block and thrust sheet rotations in the Central Northern Calcareous Alps deduced from two pervasive remagnetization events, *Tectonics,* **26,** TC5011–TC5036.

Remacha, E. & Fernández, L.P., 2003. High-resolution correlation patterns in the turbidite systems of the Hecho Group (South-Central Pyrenees, Spain), *Mar. Petrol. Geol.,* **20,** 711–726.

Remacha, E., Arbués, P. & Carreras, M., 1987. Precisiones sobre los límites de la secuencia deposicional de Jaca. Evolución de las facies desde la base de la secuencia hasta el techo de la arenisca de Sabiñánigo, *Bol. Geol. y Min.,* **98**, 40–48.

Ríos Aragüés, L.M., Galera Fernández, J.M. & Barettino Fraile, D., 1987a. *Mapa Geológico de España a escala 1:50 000. Hoja 145 (Sallent),* IGME.

Ríos Aragüés, L.M., Galera Fernández, J.M. & Barettino Fraile, D., 1987b. *Mapa Geológico de España a escala 1:50 000. Hoja 146 (Bujaruelo),* IGME.

Ríos Aragüés, L.M., Lanaja del Busto, J.L. & Frutos Domingo, E., 1972. *Mapa Geológico de España a escala 1:50 000. Hoja 178 (Broto),* IGME.

Roberts, A.P., Cui, Y. & Verosub, K.L., 1995. Wasp-waisted hysteresis loops: mineral magnetic characteristics and discrimination of components in mixed magnetic systems, *J. geophys. Res.,* **100**(B9), 17 909–17 917.

Rodríguez, L., Cuevas, J. & Tubía, J.M., 2014. Structural Evolution of the sierras interiores (Aragón and Tena Valleys, South Pyrenean Zone): tectonic implications, *J. Geol.,* **122,** 99–111.

Rodríguez-Méndez, L., 2011. Análisis de la estructura varisca y alpina en la transversal Sallent-Biescas (Pirineos centrales, Huesca), *PhD thesis,* Universidad del País Vasco.

Rodríguez-Méndez, L., Cuevas, J. & Tubía, J.M., 2013. Geological map of the central Pyrenees between the Tena and Aragon valleys (Huesca), *J. Maps,* **9,** 596–603.

Rodríguez-Pintó, A., Pueyo, E.L., Pocoví, A., Ramón, M.J. & Oliva-Urcia, B., 2013. Structural control on overlapped paleomagnetic vectors: a case study in the Balzes anticline (Southern Pyrenees), *Phys. Earth planet. Inter.,* **215,** 43–57.

Schwartz, S.Y. & Van der Voo, R., 1983. Paleomagnetic evaluation of the orocline hypothesis in the central and southern Appalachians, *Geophys. Res. Lett.,* **10,** 505–508.

Schwarz, E.J., 1963. A paleomagnetic investigation of Permo-Triassic redbeds and andesites from the Spanish Pyrenees, *J. geophys. Res.,* **68,** 3265–3271.

Séguret, M., 1972. *Etude tectonique des nappes de series décollées de la partie centrale du versant sud des Pyrénées, Caractère synsédimentaire, rôle de la compression et de la gravité,* Publ. USTELA. Ser. Geol. Struct. 2, Univ. des Sci. et Tech. Du Languedoc, 155 pp.

Soto, R., Casas-Sainz, A.M. & Pueyo, E.L., 2006. Along-strike variation of orogenic wedges associated with vertical axis rotations, *J. geophys. Res.,* **111,** B10402, doi:10.1029/2005JB004201.

Soto, R., Casas, A.M., Villalaín, J.J. & Gil-Imaz, A., DelRío, P. & Fernández, G., 2011. Integration of surface and subsurface data, paleomagnetism and analogue modelling to reconstruct the extensional geometry of the Cameros basin (N Spain), *Trabajos de geología,* **30,** 235–240.

Souquet, P., 1967. Le Crétacé supérieur sudpyrénéen en Catalogne, Aragon et Navarre, *PhD thesis,* Univ. de Toulouse, Toulouse, France.

Stamatakos, J. & Hirt, A.M., 1994. Paleomagnetic considerations of the development of the Pennsylvania salient in the central Appalachians, *Tectonophysics,* **231,** 237–255.

Stamatakos, J., Hirt, A.M. & Lowrie, W., 1996. The age and timing of folding in the central Appalachians from paleomagnetic results, *Geol. Soc. Am. Bull.,* **108,** 815–829.

Sussman, A.J. & Weil, A.B., 2004. Orogenic curvature: integrating paleomagnetic and structural analyses, *Geol. Soc. Am. Spec. Pap.,* **383,** 258.

Sussman, A.J., Butler, R.F., Dinarès-Turell, J. & Vergés, J., 2004. Vertical-axis rotation of a foreland fold and implications for orogenic curvature: an example from the Southern Pyrenees, Spain, *Earth planet. Sci. Lett.,* **218,** 435–449.

Szabó, E. & Cioppa, M.T., 2012. Multiple magnetizations in Ordovician–Devonian carbonates in the Williston Basin (Manitoba, Canada), *Geol. Soc. Lond. Spec. Publ.,* **371,** 107–122.

Taberner, C., Dinarès-Turell, J., Giménez, J. & Docherty, C., 1999. Basin infill architecture and evolution from magnetostratigraphic crossbasin correlations in the southeastern Pyrenean foreland basin, *Geol. Soc. Am. Bull.,* **11,** 1155–1174.

Tauxe, L., 2008. *Essentials of Rock and Paleomagnetism,* University of California Press.

Tauxe, L., Mullender, T.A.T. & Pick, T., 1996. Potbellies, wasp-waists, and superparamagnetism in magnetic hysteresis, *J. geophys. Res.,* **101,** 571–583.

Teixell, A., 1992. Estructura alpina en la transversal de la terminación occidental de la Zona Axial pirenaica, *PhD thesis,* Univ. de Barcelona, Barcelona, Spain, 252 pp.

Teixell, A., 1996. The Ansó transect of the southern Pyrenees: basement and cover thrust geometries, *J. Geol. Soc. Lond.,* **153,** 301–310.

Teixell, A., 1998. Crustal structure and orogenic material budget in the west central Pyrenees, *Tectonics,* **17,** 395–406.

Teixell, A. & García Sansegundo, J., 1989. *Mapa Geológico de España a escala 1:50 000. Hoja 118 (Zuriza),* IGME.

Teixell, A., García Sansegundo, J. & Zamorano, M., 1989. *Mapa Geológico de España a escala 1:50 000. Hoja 144 (Ansó),* IGME.

Torsvik, T.H., Briden, J.C. & Smethurst, M.A., 2000. Super-IAPD: interactive analysis of palaeomagnetic data, Available at: http://www.geodynamics.no/Web/Content/Software/, last accessed 16 February 2015.

Van der Lingen, G.J., 1960. Geology of the Spanish Pyrenees, north of Canfranc, Huesca Province, *Estudios Geologicos,* **16,** 205–242.

Van der Voo, R., 1966. Geology of the Sierra de Tendenera region, Spanish Pyrenees, province of Huesca, *Estudios Geologicos,* **22,** 61–64.

Villalaín, J.J., Fernández-González, G., Casas, A.M. & Gil-Imaz, A., 2003. Evidence of a Cretaceous remagnetization in the Cameros Basin (North Spain): implications for basin geometry, *Tectonophysics,* **377,** 101–117.

Weil, A.B. & Sussman, A., 2004. Classification of curved orogens based on the timing relationships between structural development and vertical axis rotations, in *Orogenic Curvature: Integrating Paleomagnetic and Structural Analyses,* Vol. 383, 1–17, eds Sussman, A.J. & Weil, A.B., Spec. Pap. Geol. Soc. Am.

Weil, A.B., Yonkee, A. & Sussman, A., 2010. Reconstructing the kinematic evolution of curved mountain belts: a paleomagnetic study of Triassic red beds from the Wyoming salient, Sevier thrust belt, U.S.A., *Geol. Soc. Am. Bull.,* **122,** 3–23.

Zechmeister, M.S., Pannalal, S. & Elmore, R.D., 2012. A multidisciplinary investigation of multiple remagnetizations within the Southern Canadian Cordillera, SW Alberta and SE British Columbia, *Geol. Soc. Lond. Spec. Publ.,* **371,** 123–144.